UNIVERSITY OF NAIROBI

A STUDY ON THE EFFECT OF MOUNTING PARAMETERS ON THE PERFORMANCE OF BIFACIAL SOLAR MODULES

BY

GLORIA KATUNGE MAITHYA

I56/39178/2021

A Thesis Submitted for Examination in Partial Fulfillment of the University of Nairobi's Requirements for Award of Master of Science Degree in Physics.

July 2023

DECLARATION

I declare that this thesis is my original work and has not been submitted elsewhere for examination, where another people's work has been used. This has properly been acknowledged and referenced in compliance with the University of Nairobi's regulations.

Signature…………….. .... Date…... 7/6/2023 ....

Gloria Katunge Maithya

I56/39178/2021

Department of Physics, University of Nairobi

This thesis is submitted for defense with our approval as supervisors at the University of Nairobi:

	Signature	Date
Dr. Sebastian M. Waita Department of Physics University of Nairobi, Kenya Email: swaita@uonbi.ac.ke		7th July,2023
Prof. Francis W. Nyongesa Department of Physics University of Nairobi, Kenya Email: fnyongesa@uonbi.ac.ke	……………..	July 7, 2023
Prof. Bernard O. Aduda Department of Physics University of Nairobi, Kenya Email: boaduda@uonbi. ac. ke	………………	12th July 2023

ABSTRACT

Bifacial Photovoltaic (bPV) is a technology that is fast gaining traction and has the potential to enhance overall electricity generation. Unlike conventional modules, bPV can capture the sun's rays and convert them into useful electricity from both the front and back of the module. Due to this, they have attracted attention in recent years. On the flip side, there hasn't been a lot of research carried out on these kinds of modules, particularly in developing countries like Kenya which are located in equatorial zones. The optimal elevation from the ground and tilt angle to install these modules vary from place to place. There haven't been many in-depth studies done on the cited area in the equatorial region, which is where the sun is directly overhead all year. This research fills that gap by giving a detailed look at how well bifacial modules work in equatorial zones. The main aim of this research was to see how varying the elevation above the default ground level and the angle of inclination affected the performance of bifacial solar modules. The study also looked at how different backgrounds affect how well a bifacial solar module works. Two solar modules were mounted back-to-back to form a double-sided solar module (bifacial solar cell configuration), with one facing the sky (front side) and the other facing the ground (back side). The module performance was examined at various elevations above the ground level and at different inclination angles by measuring parameters like solar irradiance, modules' temperature, current, and voltage both on the front and the back of the module. An HT304N reference cell was used to measure the amount of solar irradiance, and an HT instrument PT300N temperature sensor was used to measure the temperature of the module. Using an HT current-voltage (I-V) solar analyzer, the module's current and voltage were measured. At the optimized elevation and angle, the influence of different reflective backgrounds on the performance of the module was investigated using Metallized polyethylene terephthalate, MPET, iron sheet, and Mylar windshield sunshade as reflectors. Data was collected every day between 10.0 am and 3.0 pm. East African Time zone, EAT at an interval of 30 minutes for 2 months and 15 days between January and March. Data analysis and visualization were done using Python and Origin software. The findings revealed that the optimal installation elevation for bifacial modules within the equatorial zone will be 1.2 m with reference to ground level and at a tilt angle of approximately 30 degrees with north orientation. A direct proportionality relationship

between power output and solar irradiance was also noted. The maximum power output for the module's front side was 53.87 W at a solar irradiance of 1060.00 W/m^2, while the minimum power output was 34.30 W at a solar irradiance of 718.00 W/m^2. The highest power output for the module's backside was 4.82 W at a solar irradiance of 94.00 W/m^2. As the tilt angle increased, solar irradiance generally decreased on both sides of the module. It was determined that the front side received a maximum of 1060.00 W/m^2 of irradiance (at a tilt angle of 30º) and a minimum of 110.00 W/m^2 (at a tilt angle of 90º). The maximum irradiance was 88.00 W/m^2 at 30º and the lowest irradiance was 62.00 W/m^2 at 90º for the module's backside. The short circuit and maximum current were found to increase as solar irradiance increased, with a coefficient of determination, R^2 of about 0.97 for the front side of the module and about 0.92 for the backside. The findings additionally validated that the utilization of reflective backgrounds significantly enhances the power generation of bifacial solar panels. Metalized polyethylene terephthalate, MPET reflectors produced the most irradiance of the tested three reflector samples, followed by the Mylar sunshade and iron sheet. MPET increased irradiance by 84.62%, Mylar by 77.21%, and iron sheets by 22.95%. It was concluded that an elevation of 1.2 m above ground level and a tilt angle of 30º would be appropriate for bifacial module installation in equatorial zones. Moreover, due to its high reflectivity, the MPET reflector was recommended for usage as a reflecting surface.

ACKNOWLEDGEMENTS

I am incredibly thankful to the Lord, whose unwavering benevolence has been instrumental in enabling me to accomplish my work with great success.

I would like to extend my profound gratitude to my research mentors, specifically Prof. Francis W. Nyongesa, Prof. Bernard O. Aduda, and Dr. Sebastian M. Waita, for their enduring patience and endless support during the course of this research. I deeply appreciate their invaluable guidance, corrections, and assistance, which have shaped my research skills and taught me the art of effectively communicating and presenting my findings. Thank you so much for your constant dedication and mentorship.

I would like to thank the Chairman, lecturers, students, and staff of the Department of Physics at the University of Nairobi for providing a conducive learning environment for research and for enabling me to pursue this program.

I will be eternally thankful to the International Science Program (ISP) for providing me with a full scholarship to complete my Master's degree. A special thanks to Prof Bernard Aduda, the former Principal Investigator Project AFR: 03, Grant number 500-661-794 for initiating the process and ensuring that I was considered for the scholarship. I will be forever indebted.

It is with much gratitude that I acknowledge my two close pals, Mauwa and Sauline, for always being my support system throughout the research. I'm glad we started this journey together and that we're finishing it together. I'm eager to find out what the coming times have in store for us. I'll always be grateful to have you as my acquaintance. God's blessings on you. Special thanks to Stephen Warui and Mr. Opiyo from the Faculty of Science and Technology Workshop for their assistance in fabricating the tools utilized in this study.

Lastly, I'd like to thank my loving mother, Monica Mwende, For her unceasing expressions of support, continuous words of encouragement, and supplications. Not to mention Mr. Evans Shango, who has always been supportive and kept me in check anytime I felt like giving up.

Thank you to all, and may God bless you abundantly!

DEDICATION

This study owes its completion to the endless prayers and backing of my beloved mother, Monica Mwende, and my treasured siblings.

TABLE OF CONTENTS

LIST OF FIGURES

LIST OF TABLES

LIST OF ABBREVIATIONS AND SYMBOLS

ABBREVIATIONS

AM	Air Mass
AUX	Auxiliary
bPV	Bifacial photovoltaic
BSCs	Bifacial solar cell
DN	Direct Normal irradiance
EAT	East African Time
EIA	Energy Information Administration
EXP	Exponential
IEA	International Energy Agency
IES	Integrated Environmental Solutions
IRR	Irradiance
ISA	International Solar Alliance
ITRPV	The International Roadmap for Photovoltaic
I-V	Current-Voltage
LCOE	Levelized Cost of Energy
M	Meters
MC4	Multi-contact-4mm diameter
MPV	Mono-facial Photovoltaic
P	Power
PCE	Power conversion efficiencies

PV	Photovoltaics
PVGIS	Photovoltaic geographical information system
STC	Standard test conditions
UN	United Nations
UoN	University of Nairobi

SYMBOLS

A	Module's Area
β_{isc}	Bifaciality coefficient of open circuit current
β_{Voc}	Bifaciality coefficient of open circuit voltage
CO_2	Carbon dioxide
cos	Cosine
Δ	Change
D	Diffusivity parameter
f	Frontside
FF	Fill factor
G_{EI}	Equivalent irradiance
G_{RI}	Rear side irradiance intensity
$I_{ph\text{-}r}$	Rear side photocurrent
$I_{ph\text{-}f}$	Front side photocurrent
I	Current
I_d	Diode current
I_{mp}	Maximum power point current

I_o	Temperature dependence saturation current
I_p	light generated current
I_{RP}	Current flowing through parallel resistors
I_{sc}	Short circuit current
J_{sc}	Open circuit photocurrent
K	Boltzmann's constant
m	Diode ideality factor
η	Efficiency
$^\circ C$	Degrees Celsius
Pi	Incident Power
P_{in}	Power in
P_{max}	Maximum power
P_{out}	power out
q	Electric charge
r	Rear side
Si	Silicon
T	Temperature
v	Terminal voltage
V	Voltage
V_{mp}	Voltage at the maximum power point
V_{oc}	Open circuit voltage
V_{oc}	Open circuit voltage

W   Watts

W/m^2 Watts per meter squared

CHAPTER ONE: INTRODUCTION

1.1: An Overview

The research context, objectives, problem statement, and importance of the study are all discussed in this chapter.

1.2: Background of the Study

Energy is critical to meeting basic social needs, propelling economic growth, and fostering human development, and as such, it remains at the heart of every challenge and opportunity that the world faces in the twenty-first century (Wu *et al.*, 2016). This can apply to jobs, security, or food production. Population growth is one of the factors driving global energy demand and consumption. By 2050 energy demand is expected to increase by 50% (Kahan and EIA, 2019). At present, energy production that comes from non-renewable resources, such as natural gas, petroleum, and coal, constitutes 87 percent of the overall energy output. Fossil fuels are currently a key factor in the world's economic system and industrial progress, in contrast, fossil fuels are non-renewable and unsustainable energy sources with emission of greenhouse gases which have negative impacts on the environment. It is anticipated that there will be an imbalance between the demand and availability of fossil fuels, potentially leading to conflicts and economic crises around the world as fossil fuels deplete between 2069 and 2088 (Stephens *et al.*, 2010).

The consumption of fossil fuels has an adverse effect on the environment, contributing to the release of greenhouse gases like carbon dioxide, the decimation of habitats, alterations in climate trends, an increase in sea levels, the melting of glaciers, and so forth (Stein *et al.*, 2021). Subsequently, international entities such as the United Nations have advocated for a gradual shift to environmentally-friendly energy sources. The primary source of renewable energy is solar radiation. Wind, hydropower, geothermal, solar thermal, ocean energy, and tidal energy are some of the other sustainable energy sources. The appeal for renewable energy stems from its numerous benefits, which include: sustainability, abundance, supply security, no or minimal air pollution, no green gas emissions, and long system life (Deline *et al.,* 2017).

Photovoltaics (PV) and thermal collectors are the two primary forms of solar energy technology. Photovoltaic technology converts the energy of the sun into electrical power, whereas thermal collectors convert sun energy into heat. Photovoltaics has become increasingly popular as a

renewable energy source due to its low-maintenance requirements., silent, and produces clean energy (Goswami, 2017). At the moment, the most common PV devices are made of silicon and are mono-facial modules, which means they can only generate electricity when exposed to sunlight via the front surface. However, bifacial modules have been around since the 1960s and they have garnered attention in the solar PV industry because of their ability to capture photons from both direct incidents and reflected light reaching the module's front and backsides at the same time. (Kahan & EIA, 2019). According to Guerrero-Lemus *et al*., (2016), power generation can be increased by nearly 50% when the module can capture sunlight from both sides of the module and a concentrating device that increases albedo radiation is used.

The objective of this study is to assess the performance of bifacial solar modules in equatorial regions and determine optimal conditions for maximizing their power output. The investigation focuses on identifying influential factors, including module elevation above the ground and inclination angle, that affect the power yield of bifacial modules. The ultimate goal is to enhance the power generation potential of these modules by optimizing these parameters.

1.3: **Statement of the Problem**

Bifacial modules have revolutionized the field of PV energy. While their notable advantage lies in their ability to capture sunlight from both sides, their main drawback is the higher cost attributed to the double glass construction. Nevertheless, one promising approach to mitigate this cost is by enhancing the module's power-generating efficiency. By improving efficiency, it becomes possible to offset the initial expenses associated with bifacial modules, making them a more cost-effective solution in the long run. This is advantageous because higher efficiency means that fewer modules are needed to achieve the desired power output. However, the efficiency of power generation is affected by several elements, including irradiance, ground albedo, tilt angle, the structure's increased height above the ground, and array shading, among others. This study looks into the performance of these bifacial modules in the equatorial zone in terms of elevation and angle of inclination, which are key aspects to consider while placing this module in the equatorial zone.

1.3.1: Justification of the study

The optimal mounting parameters for solar modules are determined by a variety of elements such as solar irradiation, temperature, and wind speed. Because equatorial regions have unique environmental conditions, determining the most effective mounting configurations that can withstand these conditions and maximize energy output is critical. The information gathered will provide a good basis for application of bifacial technology within the equatorial zones.

1.4: **Objectives of the Study**

1.4.1: **General Objective**
To investigate the performance of bifacial modules under various mounting situations, such as inclination angle and elevation.

1.4.2: **Specific Objectives**
To determine:
1. The best elevation for the performance of bifacial modules.
2. The best angle of inclination for module performance.
3. The impact of putting a reflecting surface on the backside of bifacial and analyze its effects on module performance

1.5: **Significance of the Study**
The escalating need for power, coupled with global development, has prompted a shift towards renewable energy sources that have a lower environmental footprint. With fossil fuels currently supplying over 87% of the world's energy demand, their diminishing availability has spurred a heightened interest in solar power, as well as other renewable sources like wind and tidal energy. Solar energy, exemplified by its increasing adoption and potential in Kenya and numerous other tropical countries, offers an affordable, eco-friendly, and dependable power solution.

The current solar modules in the market has some restrictions in that, unlike bifacial modules, they can only generate electricity on the front side. This is one of the primary reasons why bifacial modules will be the next big thing in the solar business; they can produce more energy than mono-facial modules, and because it is a new technology, it is growing quickly, which may lead to its broad use in the near future.

The purpose of this research is to look at potential improvements in bifacial module performance by optimizing module elevation and tilt angle of inclination. Furthermore, the study will look into the use of reflecting surfaces to boost backside production, which generally receives less sunlight but benefits from the reflected light and albedo. Moreover, the project intends to analyze the modules' commercial viability in Kenya, as well as their appropriateness for wider application throughout Africa.

CHAPTER TWO: LITERATURE REVIEW

2.1: Overview
Earlier work on bifacial solar modules is covered in depth throughout this chapter.

2.2: An Overview of Bifacial Solar Modules
The Earth is already acknowledged as a planet facing serious energy problems, global climate change, and environmental pollution (Ma *et al*., 2018). In light of these challenges, the adoption of renewable energy sources, particularly photovoltaics (PV) since solar energy is abundant, has been recommended as a viable option. (Chen *et al*., 2019). Over the recent decade, the worldwide PV sector has risen quickly, with roughly 505 Gigawatts of global photovoltaic system circulative installations outlined in 2018 (REN21 Renewable 2019 report). As a result of these circumstances, commercial and academic interest in crystalline silicon cells has shifted from mono-facial to bifacial technology, with bifacial usage rising from less than 15% in 2019 to an estimation of 70% in 2030, according to the report shown in Figure 2.1 (Paliozian and Tepner, 2020).
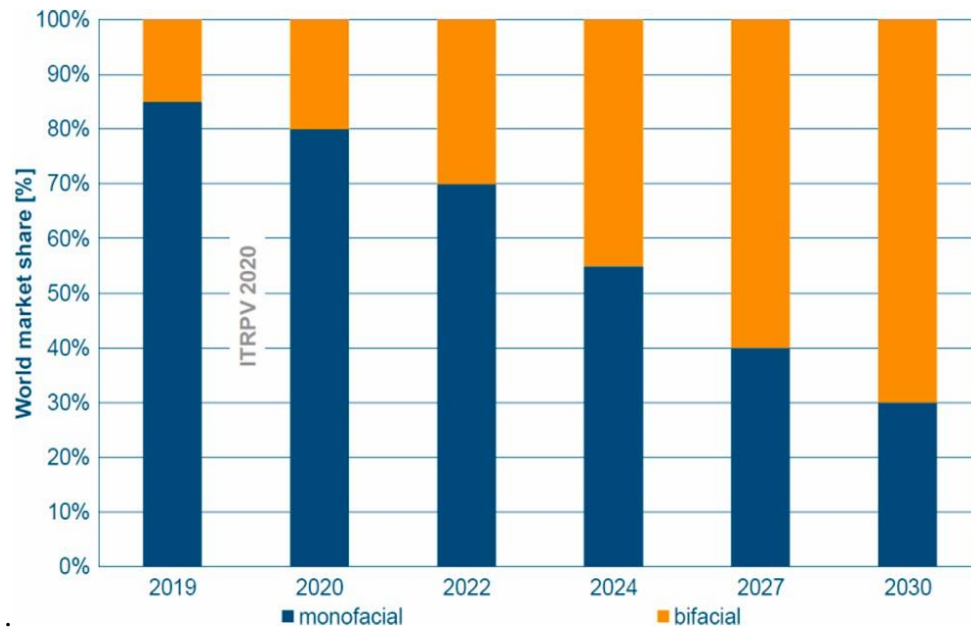
Figure 2.1: PV market development trends(Paliozian and Tepner, 2020)

The first bifacial laboratory cell according to Guerrero-Lemus *et al*., (2016) was built and presented in 1977, and each year since then, few studies concerning high efficiency and real-world applications have been published, as shown in figure 2.2. Articles regarding bifacial technology

began to rise in 2009 since people had not come to full realization of the potential behind this technology and due to that researchers over the world began to work on this unique technology, particularly in China, the United States, Germany, and Japan since they are the major players in the photovoltaic sector. Researchers have been successful in developing a bifacial PV module, which research has proven to be effective in reducing the Levelized Cost Of Energy (LCOE) associated with solar photovoltaics while simultaneously increasing the amount of energy that can be generated from the surface area it is mounted on. (Yakubu *et al*., 2022). Since bifacial PV technology can gather solar radiation by converting light into energy from both sides of the module, the energy potential of bifacial PV modules is greater than those of traditional modules. Kreinin et al. (2010) evaluated the key factors that influence rear irradiance and its contribution to energy generation for bifacial modules. These characteristics include the inclination angle, ground clearance, varying seasons of solar direction, and albedo.
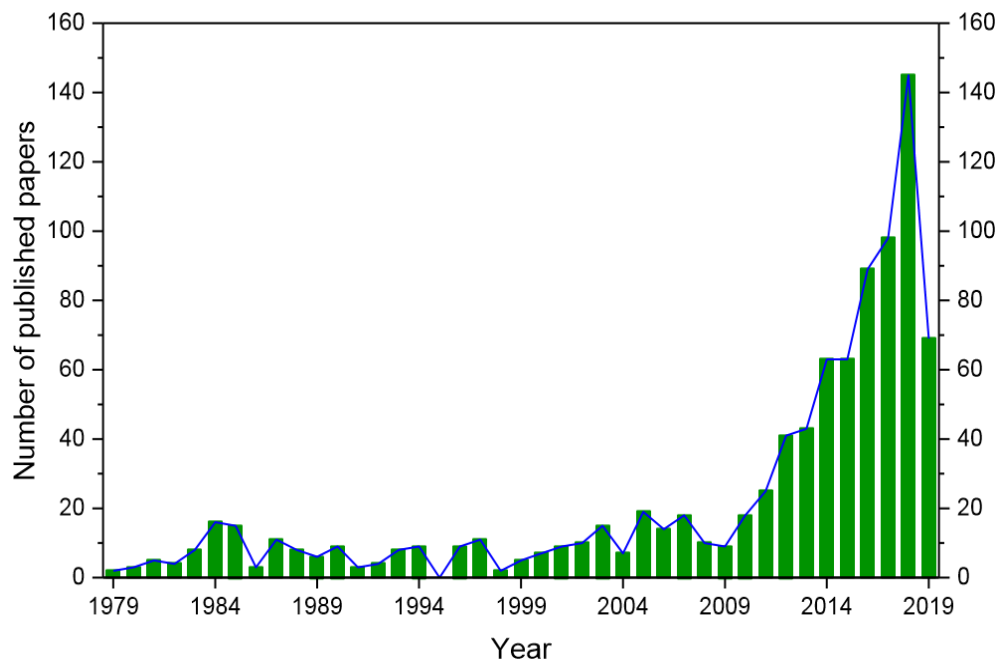
Figure 2.2: Articles published from 1979 until August 2019 on bifacial module technology (Gu et al., 2020)

According to the findings of the researchers, the amount of power generated by bifacial PV systems is thirty percent more than that generated by mono-facial PV systems when the albedo is 0.5 and the height is 1 meter (Sun *et al*., 2018). If the latitude is higher than thirty degrees, bifacial PV technology not only produces more power, but its unique features also result in a two to six percent

reduction in the LCOE (Patel *et al*., 2019). From a worldwide viewpoint, Rodrguez-Gallegos *et al*., (2018) argued that, in two circumstances, bifacial is a more cost-effective PV technology: (1) latitudes greater than 40 degrees, regardless of albedo, and (2) latitudes less than 40 degrees, but with a high albedo (Yu *et al*. (2016) conducted additional tests to estimate bifacial performance. Bifacial modules were used in convectional PV systems with a variety of tilts, heights, orientations, and tracking algorithms in a study by Stein *et al.,* (2018). The results reveal that bifacial modules outperform mono-facial modules and that they perform better when albedo rises and ground shading falls. According to an outdoor bifacial modules experiment done by Wei *et al*., (2016.), it was shown that, on sandy and snowy terrain, high albedo is useful for obtaining substantial power output improvements of up to 15% and 30%, respectively. There have been few scientific kinds of research on bifacial technology, including simulations and experiments.

Despite the many benefits it provides, the deployment of this technology has been limited due to the lack of proper modeling tools for bifacial solar modules. To accurately forecast the energy output and efficiency of these modules, it is crucial to comprehend the impacts of mounting characteristics such as ground albedo, inclination angle, raised structure height above the ground, and array size in establishing the optimal installation parameters.

2.3: Factors Influencing Performance of Bifacial Modules

There are a variety of distinguishing features that influence the bifacial performance, as illustrated in Figure 2.3. According to Van Aken and Carr (2014), some of these parameters include the location of the sun, dirtying, shadowing, dissipation coefficient, ground albedo, angle of inclination, row spacing, and the orientation of the module with reference to the sun. This section will look into a few key themes in greater depth.
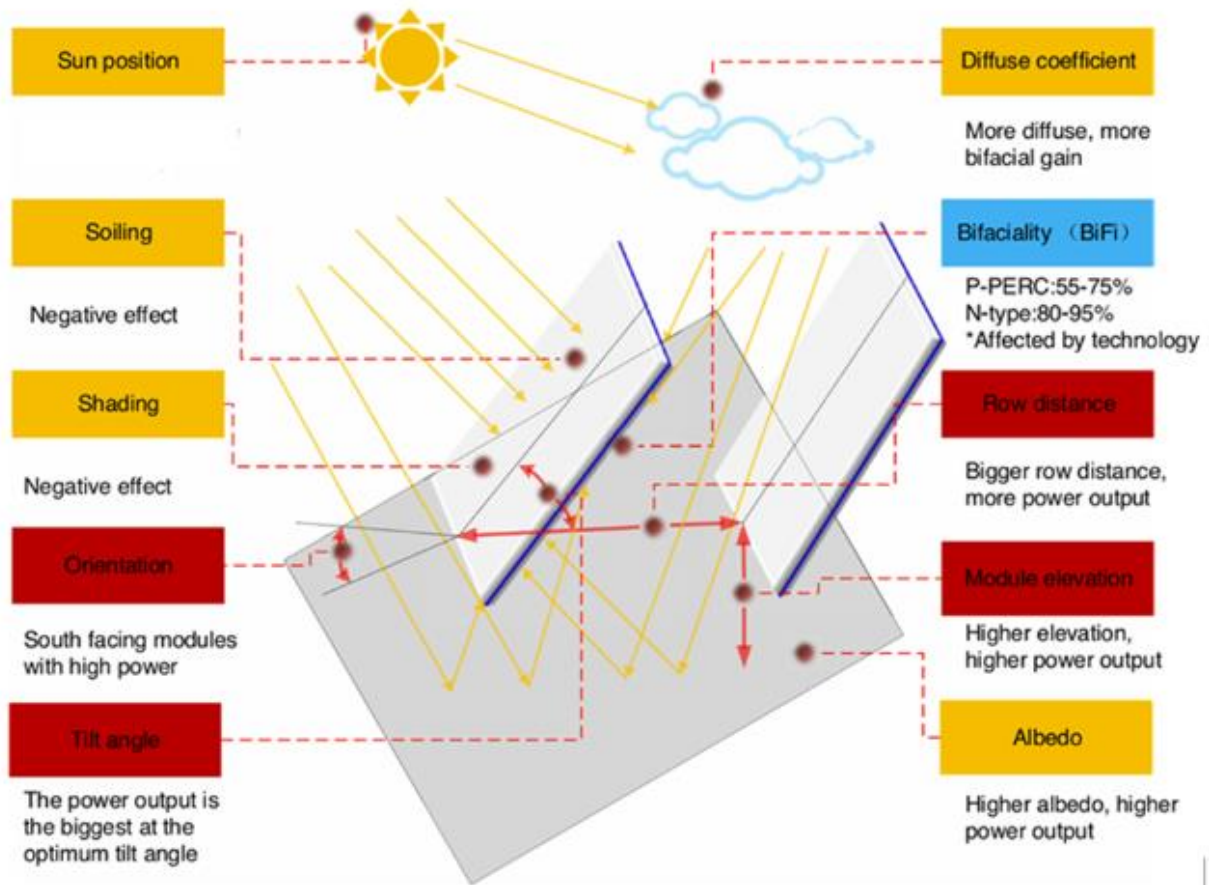
Figure.2.3: Various factors that influence the performance of bifacial PV modules (Gu et al., 2020)

2.3.1: **Albedo effects on Bifacial Module Characteristics**

Ground reflection has a large influence on rear irradiance. High rear irradiance is caused by a high albedo, which results in increasing bifacial energy output, as shown by Van Aken and Carr, (2014). As the front irradiance remains relatively constant, the bifacial gain grows linearly with albedo (Gu et al., 2020). Yusufoglu and his coworkers, (2014) modeled how energy may be produced from bifacial modules by adjusting ground reflection (albedo). According to the findings of the research, the optimal tilt angle rose when the modules were installed at closer distances to the ground. This is because the optimal tilt angle, which varies depending on the height of the module, is directly related to the albedo coefficient. The study also found that when bifacial modules are placed with their mono-facial modules counterparts in a highly reflective ground, they can generate up to 30% more energy. Either, this module can work so well in areas dominated by low-light conditions. For grass, sand, and snow, the bifacial gain can be as high as 7.6 percent, 15.4 percent, and 29.2 percent, respectively (Wei *et al.,* 2016). As a result, bPV technology can take full

advantage of high-albedo locations to create more energy (Wang *et al*., 2019). However, these studies do not inform us how we can improve the reflectivity of those radiations.

2.3.2 **Effects of elevation on Bifacial Module Features**

As the module's bifacial energy production is proportional to the module's backside irradiation, the bifacial energy output fluctuates with altitude. Salloom *et al*., (2018) in their work on the global perspective of optimizing a bifacial solar module, the study reveals that several researchers have reported on the experimental and numerical performance of bifacial modules when they are facing south-north. These studies have pointed out that, the elevation and tilt orientation of a module plays a big role in dictating the amount of energy a bifacial module can yield. At higher altitudes, bifacial energy production and bifacial gain increase at a low but steady pace as a result of more reflected irradiance from the ground and reduced self-shading (Deline *et al.,* (2016). In light of this, Yordanov et al. (2012) suggested positioning bifacial modules at an elevation of 0.5 to 1.5 meters above the ground to strike a good balance between the amount of electrical gain produced and the total area covered.

When the elevation of a bifacial module is increased, so does the amount of radiation reflect on the backside of the module. However, this increase is not linear; research has found that between 0 and 1 m in height, the power gain from the back significantly rises. After 1 m the gain slows down. This is because an increase in the height does not necessarily boost the performance of the module since self-shadowing on the backside irradiance is diminished (Asgharzadeh *et al*., 2017).

2.3.3: **Effects of Tilt Angle on Bifacial Module Characteristics**

Tilt angle, in addition to albedo, has a considerable impact on bifacial performance. The amount of energy produced each year, especially for bifacial and conventional modules, rises until they reach their optimal angles, at this point the energy rapidly decreases. The optimal angle of inclination for bifacial modules is higher than that for mono-facial modules when the same conditions are applied (Sun et al., 2018). The energy yield on the backside is less impacted by the tilt angle than on the front side. The total bifacial energy yield is calculated by ignoring the effects of scattering and diffusion on the amount of light that reaches the surface of the module. When tilted to a great degree, the substantial bifacial gain explains why vertical bifacial technology is preferred in specific applications, such as building facades (Gu, Ma, Li, *et al.,* 2020). This research

also showed that when the size of the array grew larger, the performance of the bifacial module decreased. The study, however, did not specify the ideal tilt angle for placing a bifacial module.

The effect of ambient temperature on the energy production of bifacial solar modules was investigated by Salloom et al. (2018) as part of their study evaluating the efficiency of bifacial photovoltaic panels. The open circuit photocurrent density, denoted by the symbol "J_{sc}," and the open circuit voltage (Voc) were two of the factors evaluated in the study. V_{oc} and J_{sc} for both the front and backsides dropped as the tilt angle increased in this study. Either way, the study found that as the tilt angle increased, so did the irradiance and temperature.

2.3.4: **The influence of orientation**

Because the received irradiance is affected by the orientation, bifacial PV performance varies substantially (Sun *et al*., 2012). To assess the impact of direction with sufficient precision, both static and moving cases are investigated. Due to increased irradiation, bifacial and mono-facial modules using tracking technology produced higher electricity when compared to static modules. However, tracking technology is more effective at reducing front-side irradiation than it is at reducing backside irradiance, as a result, tracking systems did not contribute significantly to the bifacial gain. The modules were mounted south in the fixed case for a higher energy yield. The modules provide a slightly lower energy production in the direction of east or west, but with a significant bifacial gain, demonstrating that bifacial technology is more versatile than mono-facial in terms of orientation.

H. Mori developed the first bifacial solar cells in 1960 (Goss, 1983). The primary goal of the production was to improve surface passivation and increase long-wavelength photon collection efficiency (Durusoy, 2020). According to the results of experiments conducted during the Soviet Union's first space station program, rear-side irradiance contribution was 10-20% depending on the orientation (Khan and Alam, 2015). The ground reflectance has a significant impact on the additional irradiance that is received from the rear side. To examine the differences between a flat module and a bifacial module, tests were carried out in a location with an extremely high ground reflectance. As a result, the bifacial modules generated 42-63% more power than flat modules (Kang *et al*., 2016). The bifaciality factor, or ratio, is what determines how much extra energy the rear side will produce. The bifaciality factor may be represented as a percentage for the nominal

values of efficiency, output power, short-circuit current, and operating voltage. (Durusoy *et al*., 2020).

The bifaciality factor is a key metric for estimating the backside output power, yet practical conditions deviate from ideal laboratory settings. Figure 2.5 compares bifacial gain on the front and back sides of a bifacial module.
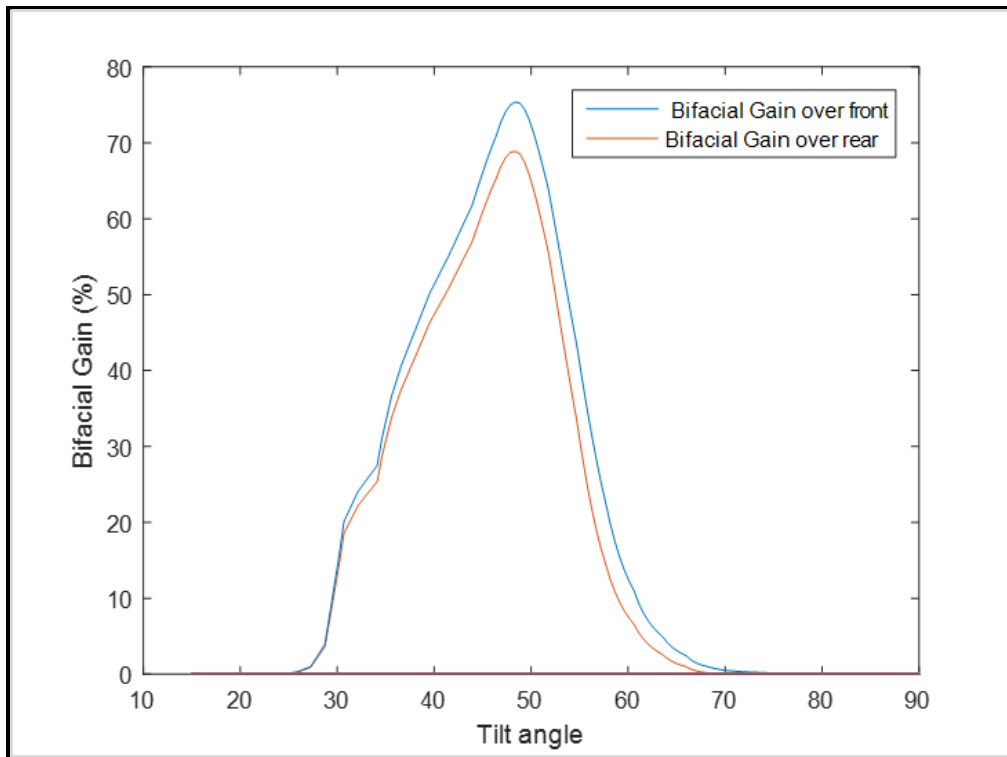
Figure 2.5: Bifacial gain on both the front and rear sides(Ademola and Qiu, 2020)

It can be seen in the Figure that the bifacial gain is smaller and more variable on the back side of the module when it is tilted. The ideal tilt angle is the same for both the front and the back, but the irradiance that is received is the primary factor that determines which side has the greater bifacial gain. The surroundings of the module have a significant impact on the amount of energy it produces, and because of this, the back of a module that is operating independently will have an excessively high level of light.

According to Guerrero-Perez *et al*., (2018), the increased amount of power that the bifacial PV module can produce is significantly affected by module installation conditions, environment, module distance with respect to the ground elevation, shadowing effects, and ground albedo. As a

result, the process of describing a model to determine the energy production of bifacial modules is more challenging than the process for mono-facial modules. Hence more research on this specific type of module is required.

2.3.5: **Effects of soiling and shading**

Soiling and shadowing have clear effects when it comes to bifacial productivity. (Bhaduri *et al*., 2019); (Luque *et al*., 2018) applied the ideas of soiling losses in power production and soiling levels to investigate the unfavorable effect that soiling has. According to the findings, vertical bifacial modules demonstrated a reduction in soiling losses as well as an overall reduction in the overall soiling level. Moreover, the bifacial module has far less soiling loss than the mono-facial module on both the front and back sides. Cleaning the backside is unnecessary because the difference between cleaning and not cleaning the backside is less than 3%, following a cleaning optimization model that was developed to direct the cleaning approach.

A study has reported that when the fill factor was increased, the shade power loss rate for bifacial modules was 12.7 percent lower than for mono-facial modules (Bhang *et al*., 2019). Furthermore, when the module is placed far behind covering it with a white object a small bifacial system loss is observed, implying that if it cannot be avoided, it is best if the white rocks are placed a distance from the PV module (De Groot and Van Aken, 2017). As a result, it can be concluded that bifacial technology demonstrated lower power loss when soiling and shading effects were present when compared to mono-facial when installed under the same installation conditions.

2.3.6: **Effects of row distance and row number on bPV**

To generate greater power, numerous bifacial modules are connected in series or parallel to form a bifacial array. Field installation parameters, such as row length and number, become a crucial factor impacting bifacial performance under these conditions (Lopez-Garcia *et al.,* 2019). Larger row spacing improves bifacial performance due to increased room background reflection, according to (Shoukry *et al*., 2016).

2.4: **Effects of Reflectors on Bifacial PVs**

For a long time, concentrators and various types of reflectors have been offered as low-cost ways to increase the quantity of incoming solar energy captured by a collector surface, hence increasing power output. Many studies on thermal collectors and mono-facial PV have been conducted. The same concept has been implemented in bifacial modules. (Riedel-Lyngskær *et al.*, 2020; Rueter *et al.*, 2021; Cha *et al.*, 2018). Reflectors have been investigated as a means of increasing power gain because the bifacial gain is solely determined by how much light is reflected onto the module's rear side. In this case, other variables such as the spacing between the collector and the reflector, the height, the tilt, the size, and the reflectivity of the reflector become significant. Without a reflector, the backside of the collector is often illuminated by ground reflection and sky-diffused sunlight, which plays a significant role in bifacial applications. (Rueter *et al.*, 2021). Thus, a reflector's presence would need to complement these other sources while reducing interference. Many reflector designs have been proposed, some of which are simple, such as mirrors and paints. More complicated reflectors include light-scattering elements like beads or powders, as well as changeable mirror arrays and pyramids. (Lo *et al.*, 2013). The studies show that the use of reflectors positively influences the power output of the bifacial. Although reflectors have been employed in the past and shown to positively contribute to power production, additional research is needed to investigate the contributions of various reflective surfaces to the output power of bifacial modules. So, the purpose of this research is to complement the current literature by examining the impacts of three distinct reflectors on power generation, with a focus on the tropics.

CHAPTER THREE: THEORETICAL BACKGROUND

3.1: **Introduction**

This chapter introduces the concepts of solar energy and radiation, photovoltaics, and the mono-facial and bifacial equivalent circuits. Electrical characterization is also discussed. Some of the factors that influence a module's power output are also discussed.

3.2: **Solar Energy**

The idea of photovoltaic or other techniques that transfer solar energy into useful forms of energy would not be complete without considering the basic features of the sun. These qualities include the sun's temperature, luminosity, and rotation. The Sun is spherical and made up of incredibly heated gaseous materials with a 1.39 x 10^9 m diameter that is typically 1.5 x 10^{11} m away from the Earth. It behaves exactly like a blackbody and is the source of the portion of the sun's rays that travels to Earth. The temperature of the earth's surface, which is around 6000 K, is referred to as the photosphere. (Isabella *et al.,* 2014). Satellites have measured the amount of solar radiation that reaches the surface of the earth to be 1366 ±7 W/m², as reported by Tiller (2017). This value varies slightly due to solar activity, but it remains relatively constant. On the other hand, the radiation that makes it to the surface of the earth is affected by several different factors. The amount of radiation that is received on the surface of the earth is reduced as a result of phenomena such as absorption and scattered radiation. The received radiation is also affected by local variations in the atmosphere. This includes water vapor, clouds, and atmospheric gases. Finally, the amount of solar radiation that is reflected off the surface of the earth is influenced not only by the location's latitude, but also by the season, the time of day, and the length of the day. These differences affect the total power that is received, as well as the spectral composition of the light and the angle at which the light hits the surface. (Maka and Alabid, 2022). Radiation path length in the atmosphere is determined by the degree to which light hits the surface. The Earth's position with the sun in the sky, known as air mass (AM), influences the path length (Hasegawa, 2020). Solar radiation loses some of its strength when it passes through the atmosphere of the earth. Thus, the distance traveled by sunlight is considered when calculating solar irradiance under clear sky conditions. When the sun is at its zenith (perpendicular to the point), this distance is the shortest (Oliveti *et a*l., 2014).

When the sun is directly overhead, a spectrum with an air mass value of 1 exists because the optical air mass equals 1, which is the ratio of the actual path length of sunlight to the minimum distance

(AM1). The mass of the air can be found by using equation (3.1), which is valid when the sun is at an angle with respect to the zenith.

$$AM = \frac{y}{x} = \frac{1}{\cos \theta}$$ (3.1)

where x, y, and θ are depicted in Figure 3.1. The angle created by X and Y is referred to as the zenith angle (Isabella et al., 2014). When the sun is directly overhead, air mass (AM) is equal to one, whereas air mass outside the earth's atmosphere is equal to zero (AM0), and air mass on the surface of the earth is equal to 1.5 (AM1.5). This corresponds to the spectrum of solar radiation with a zenith angle of 48.19 degrees. With a power density of 1000 watts per square meter and a temperature of 25 degrees Celsius, the standard test condition (STC) that is utilized the most frequently is AM1.5.
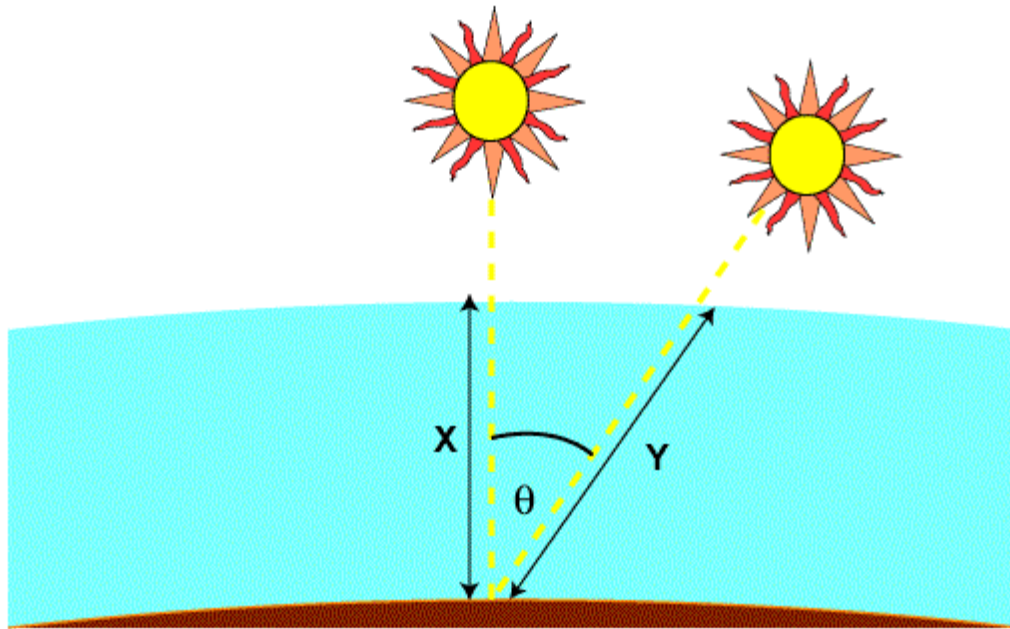
Figure 3.1: AM determination.(Yield and Estate, 2010)

Direct normal irradiance is the term used to describe the solar radiation that the earth gets when the sun is directly overhead (DN). The amount of light that is scattered or reflected by the atmosphere is referred to as diffuse irradiance (DI). Irradiance at the surface of the Earth is measured horizontally and is referred to as global horizontal irradiance (GI). and is given by equation (3.2) (Cousse, 2021)

$$GI = DI + DN * \cos(\theta)$$ (3.2)

Figure 3.2 depicts the spectrum irradiance that is present at the surface of the sun, outside of the earth's atmosphere, and on the surface of the earth itself.
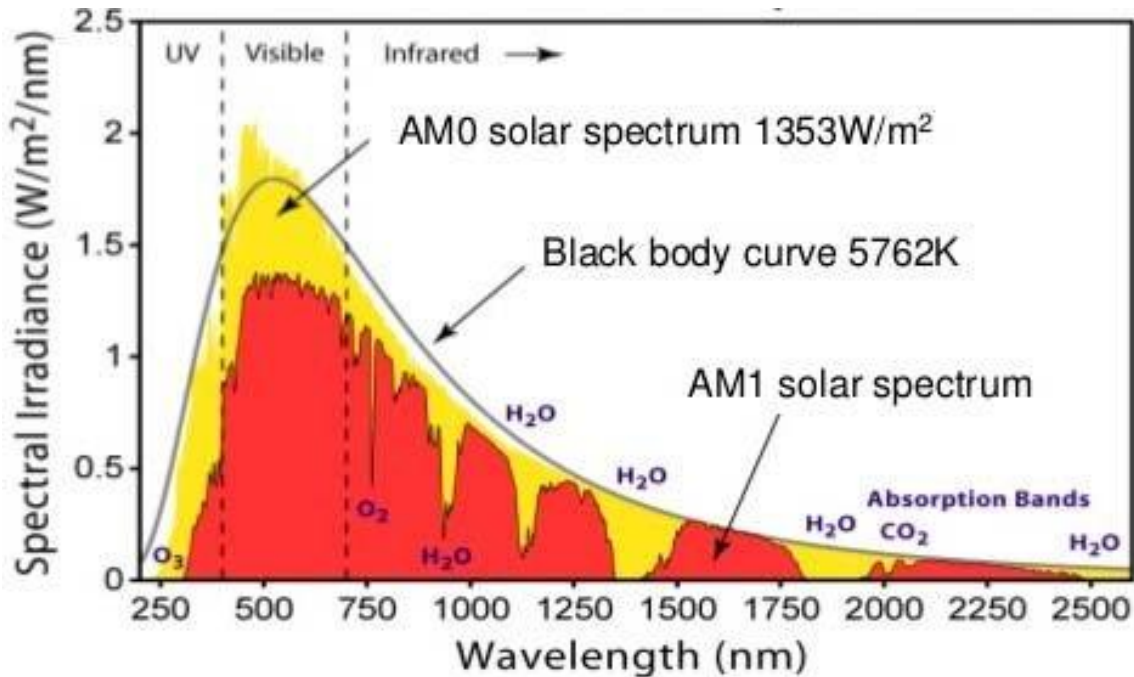
Figure 3.2 :Representation of the Spectral Distribution of Solar Radiation (Okomoli, 2019)

The spectrum has a bell-shaped pattern in the wavelength range of 0.1 - 2.5 m. As the temperature rises, often due to increased irradiance, there is a noticeable trend toward shorter wavelengths. The overall energy of the emitted electromagnetic radiation increases as body temperature rises, accompanied by a decrease in peak emission wavelength.

It is speculated that the sun's core temperature is roughly 20 million degrees Celsius. The temperature at the sun's periphery, rather than the interior, determines the electromagnetic radiation emission spectra. The estimated temperature of the sun's surface is around 6000 degrees Celsius (Okomoli, 2019).

Although radiation levels and spectral composition are constant outside the Earth's atmosphere, they vary at different latitudes and longitudes when they reach the surface. As a result, we now have a standard method for measuring the performance of devices such as solar cells, allowing us to make realistic comparisons between different locations.

3.3: Fabrication of Bifacial Photovoltaics

Solar cells with two faces, or bifacial cells, are designed to capture and convert light from the sun that falls on either side of the cell. The procedure of fabricating bifacial solar cells is significantly more straightforward than that of producing mono-facial solar cells.(Liang e*t al*., 2019). To create mono-facial solar cells, the aluminum paste is screen printed onto the back of the metal contacts, while the silver paste is applied to the front. Because this metallization process covers the back side of mono-facial cells, these cells can't generate electricity from the illumination that is received from the back side. (Luque, 1981). A bifacial PV module is made by connecting bifacial cells and covering them with a glass-like material. Figure 2.4 compares the cells and modules of mono-facial and bifacial structures. Because bifacial PV modules can capture illumination from both sides, they are more efficient than mono-facial PV modules. The effectiveness of bifacial photovoltaic systems is not only dependent on the characteristics of the cells, but also on the mounting conditions. (Guo *et a*l., 2013).
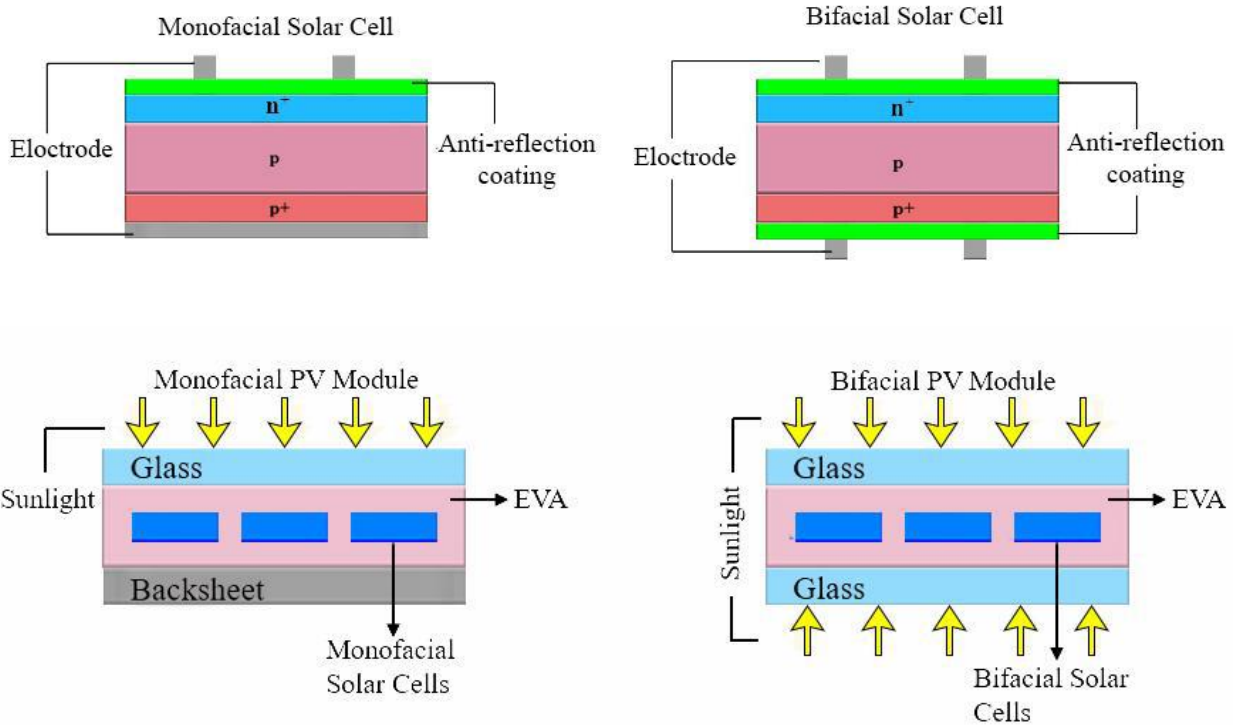
Figure 3.3: Comparing cells and modules from mono-facial and bifacial schemes(Yield and Estate, 2010)

3.4: Monofacial and bifacial PN junction Solar **Cells**

3.4.1: **How a bifacial solar cell works**

Bifacial solar cells work on the same principles as mono-facial PV technology, namely a p-n junction combined with a photovoltaic effect. A schematic representation of a p-n junction formation is shown in figure 3.3. This sort of junction is created when p-type and n-type doped semiconductor materials are joined together (Si). A p-type material has an excessive amount of holes, which results in a positive charge, while an n-type material has an excessive amount of electrons (negative charge) (Wenham et al., 2017). When p-type and n-type materials are brought together, a flow of electrons and holes begins between the two types of material.
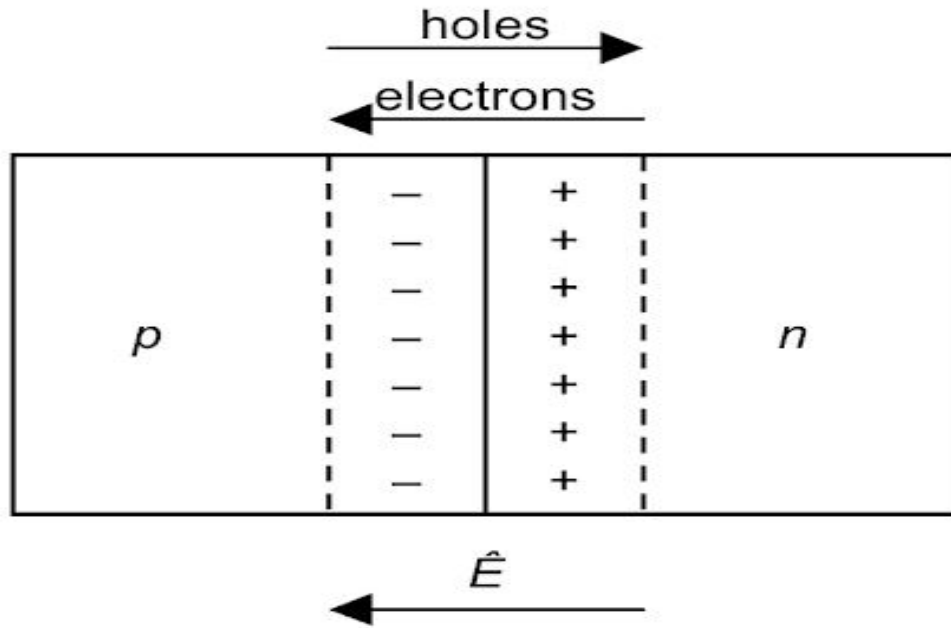
Figure 3.4:P-N junction diagram (Louw and Rix, 2020)

Therefore, a depletion layer forms as a result of the remaining exposed charges, resulting in an electric charge between the n and p-types. Applying a voltage across the junction that is high enough to overcome the electric field creates a situation where electrons and holes can flow freely and generate current. To generate an output voltage, photovoltaic cells employ photon energy from the sun to overcome the electric field at the p-n junction, resulting in the flow of current.

Bifacial cells, in contrast to mono-facial cells, have back contacts and an anti-reflection coating on the PV cells' back side. This is because, as shown in Figure. 3.4, it absorbs sunlight from all sides. Light travels through the anti-reflection coatings when solar cells are exposed to sunlight from all sides.
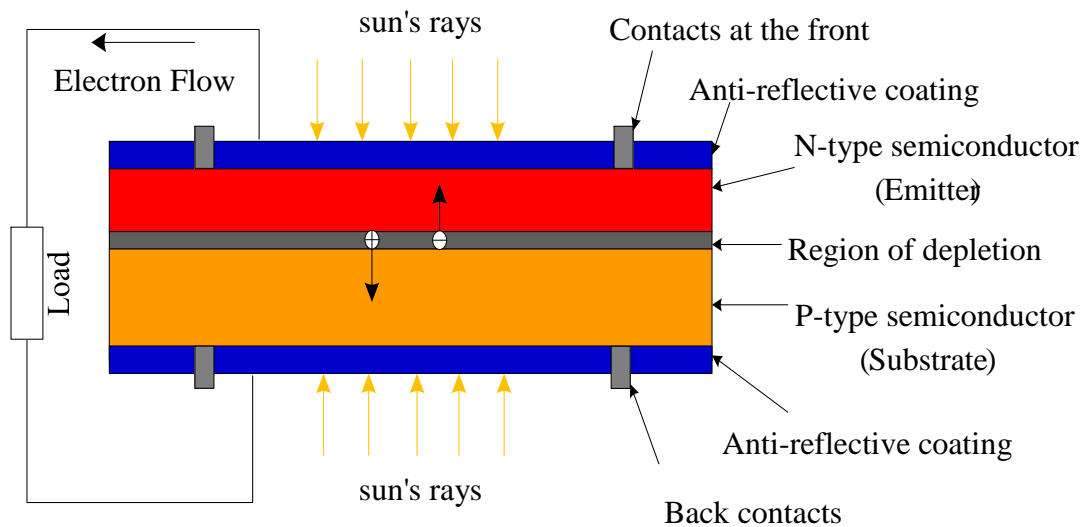
Figure 3.5: A Bifacial PV technology diagram(Lopez-Garcia et al., 2019)

A mono-facial PV module is formed when you combine a variety of separate PV cells. Most high-power output modules have 60 or 72 cells that combine to produce power output amounting from 150 to 400 W. The front and back electrodes, which are both negatively and positively charged, are two essential components of any PV cell. Since the rear electrode is connected to the p-type material, it has a positive charge. On the other hand, the front electrode has a negative charge because it is connected to the n-type material. This allows current to pass from the rear electrode to the front.

Figure 3.5 demonstrates a mono-facial PV cell design. The rear electrode is a conductive material that is opaque and wraps around the entire back of the cell. When it comes to bifacial cell design, this is where the difference lies.
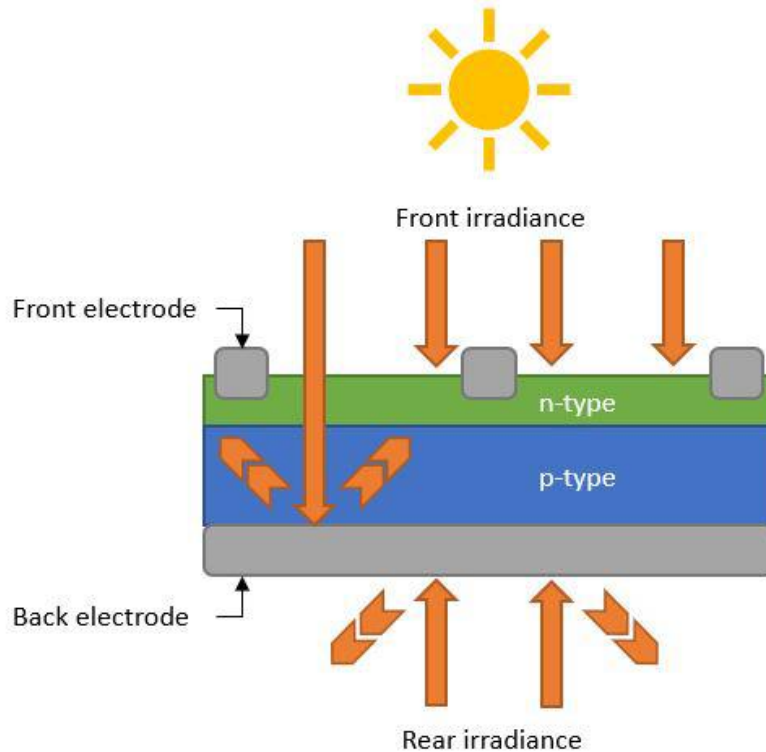
Figure 3.6: A mono-facial PV technology (Louw and Rix, 2020)

When a bifacial cell is exposed to sunlight, both front and back contacts allow radiation to pass through the cell, with the rear side receiving the reflected sunlight from the surrounding. When more radiation enters the semiconductor, more holes and electrons move between the p and n-type layers, increasing current and power output. Increased rear-side irradiation is the primary factor in the 5–30% boost in output power. (Nussbaumer *et al.*, 2020).

3.5: **Electrical Characterization**

When purchasing a PV module, among the most crucial considerations is its electrical characteristics. Unfortunately, the electrical characteristics of bifacial modules are yet to be determined due to the numerous uncertainties surrounding this new technology (Guerrero-Lemus et al., 2016). To further comprehend the limitations of bifacial module characterization, some information on the electrical characterization of mono-facial modules is provided. (Riedel-Lyngskær et al., 2020)

3.5.1: **Characterization of mono-facial PV modules**

The relationship between a single module's output current and voltage is what defines PV modules the most. These aspects of the relationship between current and voltage are referred to as the I-V characteristics. Here are some essential terms to know while discussing solar cells:

Open-circuit voltage (V_{oc})
The maximum voltage a cell can reach when no current is flowing through it. The degree of forward bias on the solar cell is reflected by the open circuit voltage. This is because the bias of the solar cell junction is caused by the current that is generated by the light. Figure 3.6 illustrates a solar cell's I-V curve.

.
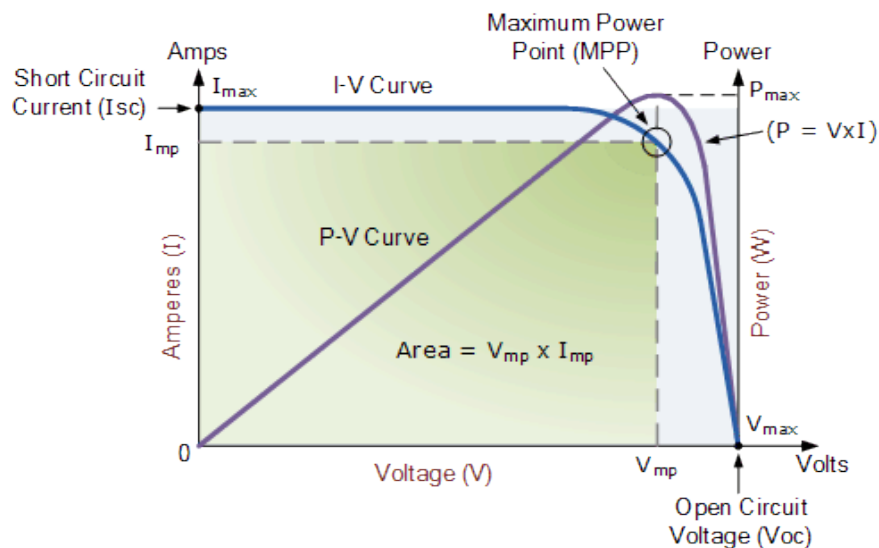
Figure 3.7: The current-voltage (I-V) curve for a solar module. (Oudira et al., 2018)

Solar irradiance is a factor that determines the open circuit voltage; conversely, an increase in temperature results in a drop in open circuit voltage. (Guerrero-Perez *et al*., 2018).

(b) Short-circuit current (I_{sc})
This is the highest current that may flow through a cell, and it occurs under no-load (voltage=0) short-circuit conditions. (Mwarabu, 2020). Short circuit current is also affected by solar irradiance in that it rises as solar irradiance rises and is directly proportional to power output. Either way temperature rise slightly increases the short circuit current (Sharma et al., 2015)

(c)The maximum power (P$_{max}$)

Maximum power refers to the maximum amount of power that the module can produce under optimal conditions without surpassing the design constraints. This is what is used to assess the PV system's performance. This specification is also gotten from the module back sheet.

Using the current–voltage (I–V) curve, one may get the power output (P) of the cell using equation (3.4).

$$P = IV \qquad (3.4)$$

In equation (3.4) above, the power scale is on the right. At the I$_{sc}$, V$_{oc}$, power equals zero. The greatest power is found between the points I$_{sc}$ and V$_{oc.}$ The voltage and current at the point of maximum power, respectively, are denoted by the symbols V$_{mp}$ and I$_{mp.}$

(d)The fill factor (FF)

Under Standard Test Conditions (STC) the open-circuit voltage of laboratory silicon solar cells is 720 mV, while the V$_{oc}$ of commercial solar cells exceeds 600 MV (Isabella et al., 2014). The FF, which may be calculated as stated in equation (3.5) below, is a measurement that compares the maximum power output of a real solar cell to the maximum power output of an ideal solar cell.

$$FF = \frac{Imp*Vmp}{Isc*Voc} \qquad (3.5)$$

A solar cell's quality is determined by its fill factor. Quality crystalline solar cells fill factor values range from 0.75 to 0.85 while for amorphous solar cells it is from 0.5 to 0.7 (Jao et al., 2016) .

(e) Efficiency (η)

To determine the efficiency of a module, just divide cell's power output, P_{out} (the rated power of the module) by its power input, P_{in} (the calculated power from the I-V curve). To achieve optimum efficiency from a solar cell, it must be operated at its maximum power output, (P_{max}). The efficiency can be calculated by the following equations (3.6) – (3.8) (Sharma et al., 2015)

$$n = \frac{FF*Voc*Isc}{solar\ power} \qquad (3.6)$$

$$\eta = \frac{Pout}{Pin} \Rightarrow \eta max = \frac{Pmax}{Pin} \qquad (3.7)$$

The most common method for calculating efficiency is to apply a P_i (incident power) value of 1000 W/m2 to the AM 1.5 formula, which can be seen below.

$$\eta = \frac{Pm}{APi} \Rightarrow \frac{FF*Isc*Voc}{APi} \tag{3.8}$$

where *A* is the module's area. The solar cell efficiency of silicon solar cells, according to (Isabella *et al.*, 2014), is between 15 and 17%.

3.5.2: **Characterization of bifacial solar module**

There has been little research on bifacial module characterization, and several approaches have been proposed (Louw and Rix, 2020). However, under IEC60904-1-2, a standardized characterization procedure for bifacial PV devices was published in January 2019 (Stefan, 2021). The steps below can be used to describe this procedure (Louw and Rix, 2020).

(a) **The Bifaciality of the module**

The Bifaciality coefficient (β), which is expressed as a percentage, is used to characterize the relationship between the production contribution of the back side of the module (γ) and the production contribution of the front side of the module (*f*) when both sides are exposed to identical illumination conditions. The three Bifaciality coefficients are $\beta_{Isc;}$ βV_{oc}, and βP_{max} as presented in Equations (3.9) – (3.12) below. It is the smallest of these three coefficients that is used to determine the bifaciality.

$$\beta I_{sc} = \frac{Isc - \gamma}{Isc - f} \tag{3.9}$$

$$\beta v_{oc} = \frac{v_{oc} - \gamma}{v_{oc} - f} \tag{3.10}$$

$$\beta^p max = \frac{P\, max - \gamma}{p\, max - f} \tag{3.11}$$

$$\beta = min[\beta Isc \cdot \beta_P max] \tag{3.12}$$

In the preceding equations (3.6)– (3.9), r denotes the module's back side and f it's front. To get the values for the above coefficients, the measurements are proposed to be taken while the front side and rear side are individually illuminated at STC (1000 W/m^2, 25 ℃, and Air Mass (AM) =1.5).

(a) **The bifacial gain of the module**

Bifacial gain refers to the increase in a module's overall output power due to back-side contributions. The International Electrotechnical commission, IEC, the standard specifies two methods for determining a module's bifacial gain (Stefan, 2021).

(1) **Double-sided illumination**- both faces must be illuminated at the same time. Illumination is provided on the back side at a minimum of three different intensities, while the front side receives 1000 W/m^2 of illumination. Then each rear side illumination's maximum power output is measured and plotted. The experiment can be done either indoors or outdoors (Louw & Rix, 2020).

(2) *One-sided illumination*- In this instance, the only part of the module that has illumination is the front, and it is lighted at three different intensities. Following the calculation of Bifaciality using the measurements, a comparison test is thereafter perfomed. This procedure is carried out in a controlled laboratory environment, and its results can be stated using the equation (3.13).

$$G_{Ei} = 1000\omega_m^{-2} + (\beta G_{Ri}) \qquad\qquad (3.13)$$

Where i =1, 2, 3…., G_{Ei} - irradiance of the three different intensies; β-bifaciality coefficient from equation (3.6) – (3.9) and G_{Ri} is the rear side irradiance calculate the equivalent irradiance (GEi), the selected rear side irradiance intensities (GRi) are first scaled down using the bifaciality, (β), and then added to the reference front side solar insolation of 1000 W/m^2 as stated in Equation 1. (3.13). This process aims to overexpose the cells with illumination that can effectively reach either of the module's faces.

(a) Illumination on both sides of the object   (b) Illumination from only one side

Figure 3.8: Different approaches that have been suggested for estimating bifacial gain. (Louw and Rix, 2020)

(b) Characterization data for Bifacial Module

Standardizing characterization process, but also the information that module manufacturers are required to report is essential. This allows PV investors to compare various modules on an equal footing. Bifacial PV devices must report the following data, according to IEC60904-1-2 (Arnoux *et al.*, 2018);

1. STC data as it relates to Mono-facial modules, i.e.

   ✓ Open-circuit voltage, V_{oc}
   ✓ Short- circuit current, I_{Sc}
   ✓ Maximum Power point, P_{max}

2. Bifaciality coefficient (β)

3. Maximum power points with contributions from the back side

   $Pmax_{\text{bifi}100}$ $(G_{Ri}=100\text{W/m}^2)$

   $Pmax_{\text{bifi}200}$ $(G_{Ri}=200\text{W/m}^2)$

The modeling of the electrical behavior of bifacial modules will be achievable once sufficient characterization data has been collected and analyzed.

3.6: **Equivalent Circuit of a Solar Module**

3.6.1: **PV module with a single face (one-diode model)**

Understanding the current-voltage curve is essential for characterizing PV modules. The I-V curve of a photovoltaic module or cell is the superposition of the diode's I-V under light and under darkness. Figure 3.8 depicts the I-V curve characteristic.
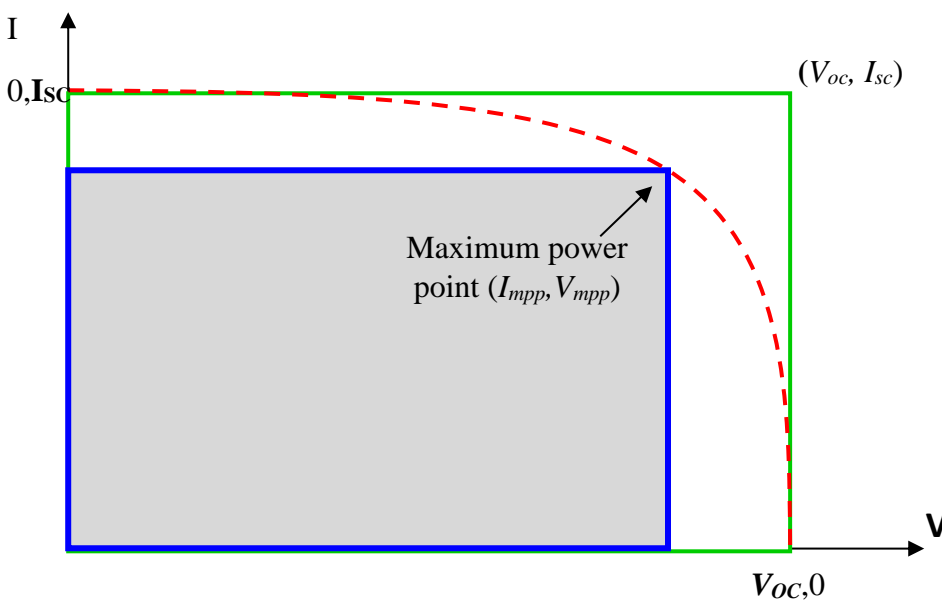
Figure 3.9 : Typical I-V curve that is representative of a solar cell. (Njagi Nguu, 2017)

Ideal solar cells, as is well known, operate in a similar fashion to a current source linked in parallel with a diode. Resistors are added to this ideal model to represent losses, and extra diodes are occasionally added to account for other phenomena. Figure 3.9 shows the most commonly used circuit for simulating a solar cell or module. It consists of a diode, a current source, and two resistors that are connected in parallel and series. (Cubas *et al.*, 2014).
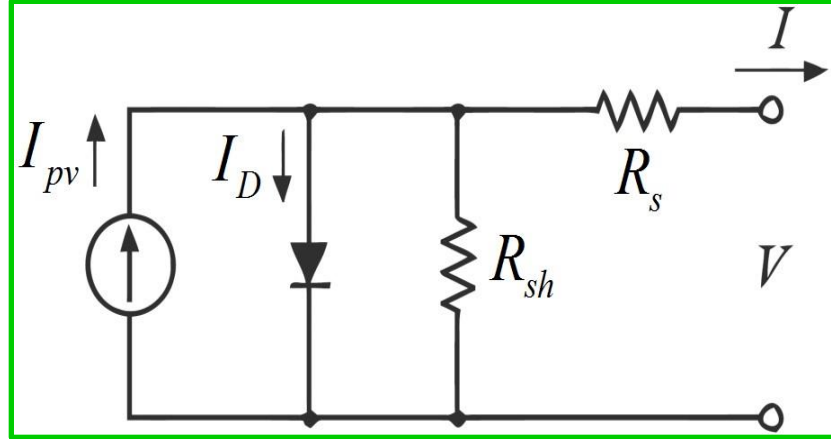
Figure 3.10: The equivalent circuit of a mono-facial module based on a model with a single diode. (Yield and Estate, 2010)

Modeling the performance of a solar cell using the standard equivalent single diode model is a frequent practice. It is based on Kirchhoff's current law, which states that the output current produced by a solar cell is equal to the photocurrent produced minus the currents generated by the parallel resistor and the diode as demonstrated by equation (3.14) (Cubas *et al*., 2014)

$$I_v = I_P - I_d - I_{RP} \qquad (3.14)$$

where I_v -the cell output current,

I_p - the light generated current (photocurrent),

I_d - diode current,

I_{RP} - current flowing through the parallel resistor.

The output current of the solar PV cell can also be expressed as shown in equation (3.15) (Yield & Estate, 2010) .

$$I = I_p - I_R\left[e^{qv/mkT} - 1\right] \qquad (3.15)$$

Where

I_d - the cell output current,

I_p - the light generated current (photocurrent),

I_R- reverse bias saturation current of diode,

q - is the electron charge,

v - is the applied voltage,

m - is the diode ideality factor,

k - is the Boltzmann's constant ($1.38*10^{-23}$J/^{0}K), and T is the cell temperature.

The open circuit voltage, abbreviated as Voc, and the short circuit current, abbreviated as Isc, are two of the most important aspects of a solar cell. When the solar cell's terminal is shorted out at constant junction temperature ,the current in a short circuit, is calculated as follows:: ((Yield and Estate, 2010)

For $V=0$, equation (3.15) above reduces to; $I = I_p$ which equals to the I_{sc}.

When the solar cell's terminal is open circuited at the constant junction temperature, the voltage in an open circuit can be written as follows:

For $I = 0$; $V = V_{OC}$

With the implication that the cell's output power is provided by;

$$p = V \left[I_{sc} - I_{Re}^{(qv/mkT)} - 1 \right] \tag{3.16}$$

When calculating the series resistance, the inverse of the slope of the current–voltage (I–V) curve at open circuit voltage is utilized. This inverse slope may be written using the equation (3.17) as shown below (Cubas *et al.*, 2014)

$$R_S = -\frac{\Delta Voc}{\Delta I_0} \tag{3.17}$$

$$R_P = -\frac{\Delta V_{oc}}{\Delta I_{sC}} \tag{3.18}$$

While Equation (3.18) indicates that it is also possible to compute the shunt resistance directly from the slope of the I-V relationship.

3.6.2: **Bifacial PV module (one-diode model)**

The one-diode model for mono-facial photovoltaic cells, known as Rsh - Rs, can be adapted to work with bifacial PV cells by adding an extra current source, denoted by Iph-r, as depicted in figure 3.9.(Libal and Kopecek, 2018). In this photovoltaic equivalent circuit, the current sources denoted by the symbols Iph-f and Iph-r each stand in for the photovoltaic contributions made by the front and backsides, respectively, as a result of the irradiance that was incident upon them. Figure 3.10 shows a one-diode model that produces equations (3.16) for output current and (3.17) and (3.18) for both front and rear photon current (I_{ph-f} and I_{ph-r}) respectively. The amounts of solar energy that hit the front and back surfaces of the bifacial cell respectively are denoted by G_f and G_r, respectively. Therefore, the obtained values for both the front and rear side solar insolation are utilized to calculate the photon current.
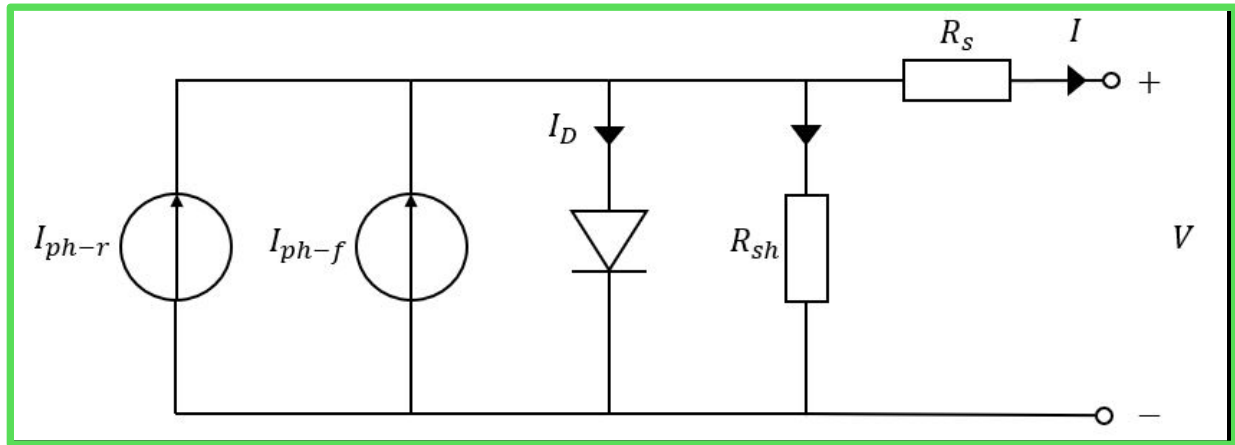
Figure 3.11: Bifacial PV cell one-diode model (Louw and Rix, 2020)

$$I = I_{ph-\gamma} + I_{ph-f} - I_0 \left[exp\frac{q(v+IR_s)}{nkT} - 1 \right] - \frac{v+IR_s}{R_{sh}} \qquad (3.19)$$

$$I_{Ph-f} = \frac{G_f}{G\gamma ef}\left(I_{sC-f} + \alpha\varDelta T\right) \qquad (3.20)$$

$$.I_{Ph-\gamma} = \frac{G_\gamma}{G_{\gamma ef}}\left(I_{sC-\gamma} + \alpha\varDelta T\right) \qquad (3.21)$$

If the values of R_{sh}, R_s, n, and I_o can be solved, a specific model for the bifacial PV cell can be developed.

Solar cells are the type of semiconductors devices that are temperature sensitive. The band gap of the semiconductor will become narrower as the temperature increases. The smaller the band gap, the higher the energy of the electrons that are contained within the material. As a result, breaking the link takes less energy. A decrease in bond energy in a bond model of a semiconductor band gap reduces the band gap, resulting in a drop in band gap with rising temperature (Foldvik, 2019).

A solar cell contains numerous components that are affected by temperature changes. The voltage measured across the open circuit is the most crucial component. Figure 3.11 illustrates how temperature affects open circuit voltage. Short circuit current increases slightly with increasing temperature, but open circuit voltage decreases, leading to a drop in maximum solar output and efficiency. (Luta, 2019).
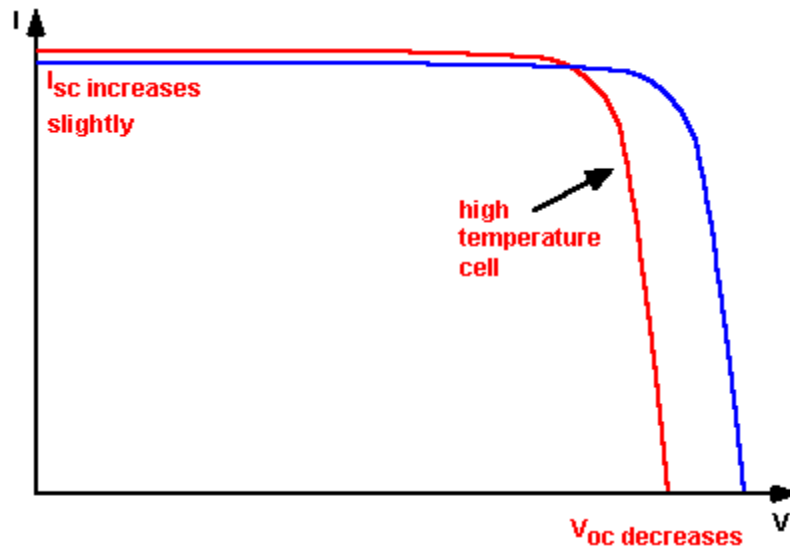
Figure 3.12: Temperature's impact on the I-V solar cell curve ((Cubas et al., 2014)

The temperature dependency of saturation current is responsible for the drop in open circuit voltage that occurs when the temperature increases (Io), which is given by equation (3.22):

$$I_0 = qA \frac{Dn_i^2}{LN_D} \qquad (3.22)$$

Where q represents the electric charge, A the area, D is the diffusivity parameter, L is the minority carrier diffuse length, N_D is the amount of doping, and n_i is the concentration of intrinsic carriers. This equation determines the amount of current that is passing through one side of a P-N junction.

CHAPTER FOUR: MATERIALS AND METHODS

4.0: Overview

This chapter explains how data was obtained and the methodology used to mount the module. The first section of the chapter describes the market sources of apparatus employed in this project. It also discusses how the tools were fabricated before their use in data collection. The chapter then goes on to explain the experimental setup before describing the data analysis procedures.

4.1: Materials Acquisition

The materials used in this work are listed below; Two polycrystalline modules, a Solar I-V analyzer, An HT304N reference solar cell, Multi-Contact-4mm diameter MC4 connectors, Calibrated angle scale, a Fabricated solar rack, Connection cables, a Multimeter, Temperature sensor, Reflective surfaces: Iron sheet, Mylar windshield sunshade, Metallized polyethylene terephthalate, and MPET reflector.

The two 60 W polycrystalline solar modules used in this work were locally sourced from Chloride Exide (K) Ltd in the Industrial Area, of Nairobi, Kenya. The solar I-V analyzer (HT), multimeter, and an HT304N reference solar cell were made available from the Solar Laboratory, Department of Physics, University of Nairobi. The MC4 connectors and connection cables were locally obtained from a local shop in Nairobi. The galvanized terrain iron sheet was acquired from local hardware in River Road, Nairobi, Kenya. The reflective Mylar windshield sunshade was bought from a local supermarket, in Nairobi. The MPET was acquired from a local designer and supplier of Heliac Solar Cooker Company. The calibrated angle scale and the adjustable solar mounting rack used in this work were fabricated at the Faculty of Science and Technology Workshop, Chiromo Campus, University of Nairobi, Kenya. The mounting rack for the module was designed in such a manner that it was capable of adjusting the elevation of the module relative to the ground level as well as changing the angle of inclination of the module. The mounting rack had a maximum elevation of 1.5 m above the default ground, and the module's tilt angle could be varied from 0º up to 90º, in 30º increments. Kenya Bureau of Standards has guidelines on mounting if monofacial modules.These guidelines were customized for bifacial in this work. The electrical parameters of the modules used in this project are presented in the table below (Table 4.1):

Table 4. 1: The electrical properties (at STC) of the 60W solar polycrystalline modules

used in this work

Maximum power, P_{max}	60W
Maximum current at the power point, I_{mp}	3.21A
The maximum voltage at the power point, V_{mp}	18V
Open Circuit Voltage, V_{oc}	22.9V
Short circuit Current, I_{sc}	3.41A
Power tolerance	± 5%

4.2: **Experimental Setup**

The experiments were carried out in three sections: The first part involved ground-level elevation optimization, the second part involved optimization of the solar module tilt angle and the third part involved the use of reflective surfaces beneath the setup. The default ground surface was concrete (concrete slab, beige). Experiments were conducted on the balcony located on the top floor of the University of Nairobi's Department of Physics, Chiromo Campus. (1.2732° S, 36.8049°, Elevation – 1698 m/5571 feet). The location was chosen due to its strategic location to the Department (closest) and its open to the sky (no shading).

Two modules, of similar characteristics, were joined together using two hinges making them foldable to cover the area of one module or spread to stretch out to cover twice the area of one module as shown in Figure 4.1. When folded, the modules could be connected in series or left each on its own creating a front (facing the skies) and back (facing the ground) side of the modules. When spread, the modules could as well be connected in series to make a 120 W module, or each module left alone to make an individual module, but both are exposed to the sun-both front.

(a)   **(b)**

Figure 4.1: The foldable modules (a) and unfolded modules (b)

To form a bifacial configuration, the two 60 W polycrystalline solar modules were placed back-to-back (one module facing up and the other facing down - the foldable model). The one facing upwards was designated the front side, while the one facing downwards was designated the backside. The calibrated angle scale was fastened to the frame of the module and was used to set the modules to various angles of inclination as in Figure 4.2.

Figure 4.2: The calibrated angle scale fitted to the module's frame.

Solar irradiance was measured using the HT304N reference cell. The reference cell has two output ports; for the Si multi-crystalline and Si monocrystalline cells. As seen in Figure 4.3, the multi-crystalline output was used as the module for this study. In this setup, the reference cell was firmly affixed in a parallel orientation to the solar module's base and clamped with a set screw to ease assembly and ensure it had the same orientation and tilt as the test module.

Figure 4.3: The HT304N Reference Cell is mounted to the module frame.

The output power of the test module was measured using the current and voltage analyzer (HT) shown in figure 4.4 by connecting the module's positive and negative terminals to the I-V analyzer.

Figure 4.4: Current-voltage (I-V) analyzer used in this study

Data from the HT304N reference cell was also recorded using the I-V solar analyzer. The data was sent from the I-V analyzer to a computer via a C2006 fiber optic connection. Figure 4.5 depicts the Top View software display when connected to the I-V analyzer.
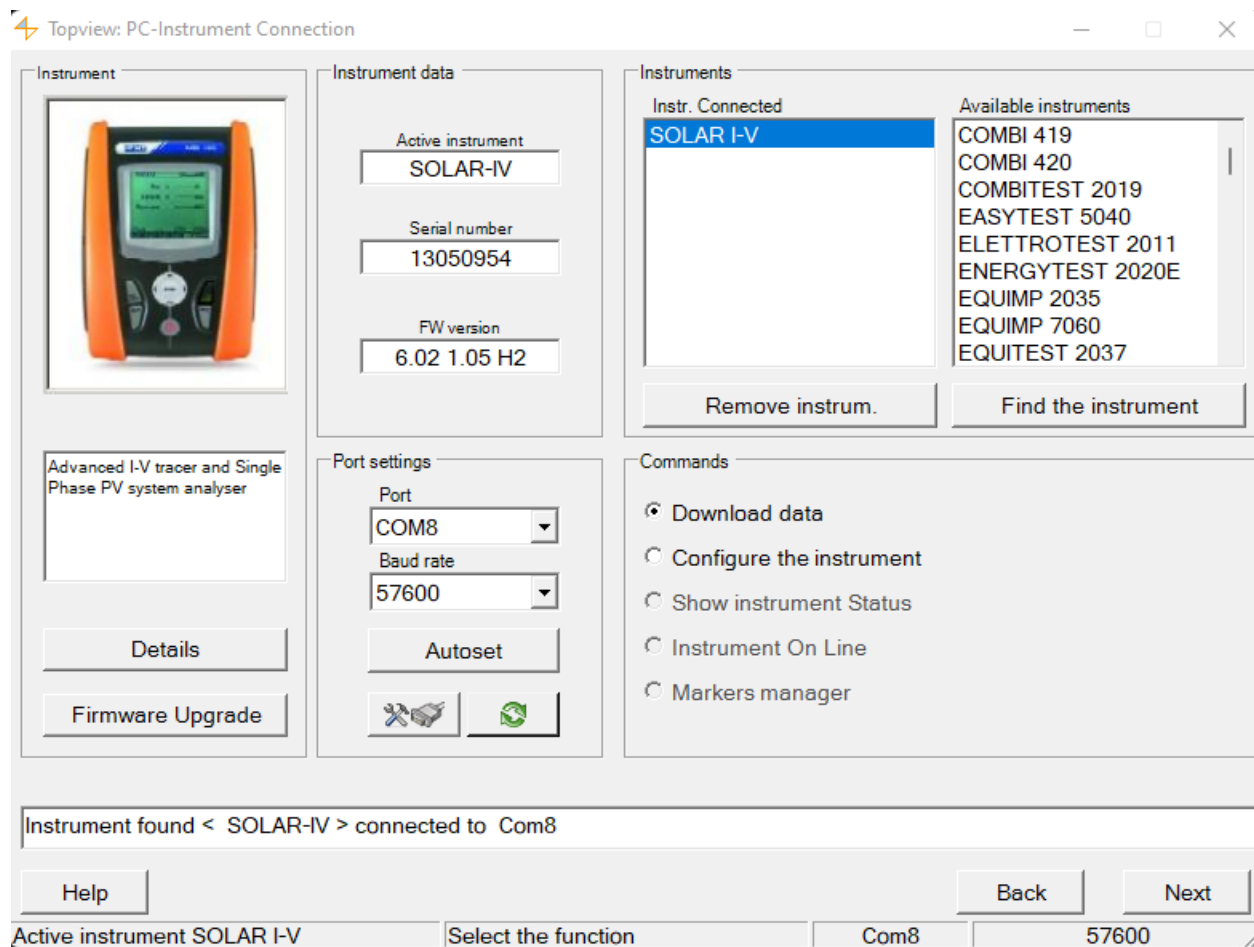
Figure 4.5: An image taken from the Top View software that is shown on the screen of a computer when an I-V analyzer is connected to that computer.

4.3: **Experimental Procedure**

Individual module characterization

Each module was first characterized by taking its I-V data after setting up the experiment as follows. The module was mounted on the mounting rack at a ground elevation of one meter from the ground and then set at an angle of 0 °, facing North. An HT304N Reference solar Cell was also mounted alongside the module and with the same inclination and orientation. Both the module and the HT304N Reference Cell were then wiped using a clean wet cloth. Current-voltage (I-V) data was gathered by connecting the module terminals to the I-V Analyzer. The irradiance probe from the HT304N reference solar cell was connected to the I-V Analyzer. The temperature sensor (HT) was fixed at the back of the module and then connected to the HT304N Reference Cell as well. The connection was used for both the front and backsides of the module depending on the focus

of measurement. Figure 4.7 (b) displays this connection. The data collection took place from ten in the morning to three in the afternoon at intervals of thirty minutes (Time in East Africa (EAT) for 2 months and 15 days and the data was analyzed using OriginPro 2021 software. Python was also used to do data analysis.

Python is a popular programming language for working with data because of the many libraries and tools available. In this project, the libraries used were Pandas, NumPy, matplotlib, and sci-kit-learn. The data collected every day, consisting of up to eleven tables, was large, and Python was used to clean and combine the tables into a single data frame. This process was repeated for all the data collected, including data on height optimization, tilt angle, and the use of reflective surfaces.

Figure 4.6 demonstrates the I-V Analyzer connections to the solar module and the reference cell.
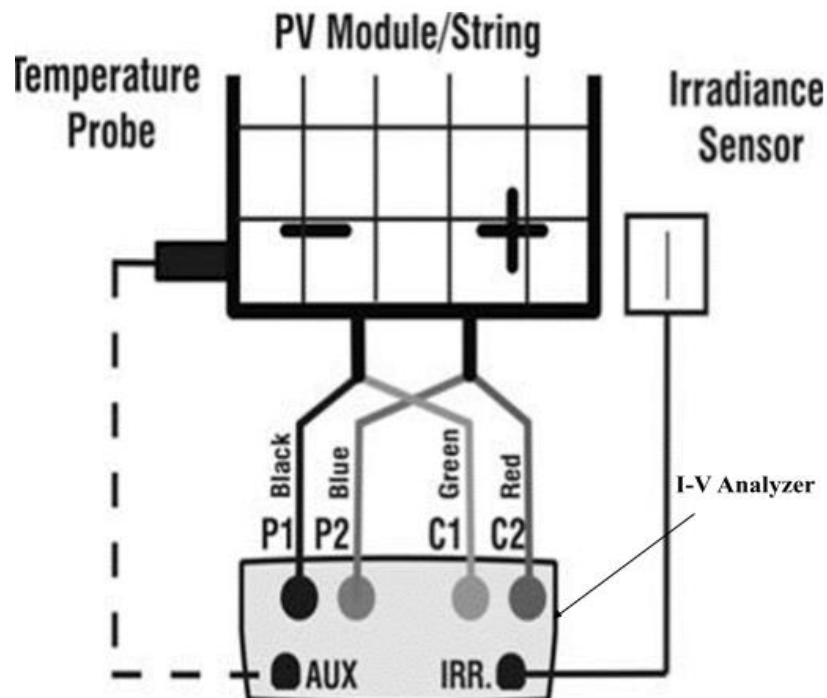
Figure 4.6.: I-V analyzer connections to the solar module and the reference cell. (https://www.ht-instruments.com/en/products/i-v400w *accessed on Nov 2021)*

The negative output of the module was connected to the P1, and C1 input terminals of the I-V Analyzer, while the positive output was connected to the P2, and C2 input terminals. The temperature sensor probe was fastened to the module's rear using scotch tape and was connected

to the auxiliary port. A connection was made between the output of the parallel (reference) solar cell and the IRR of the analyzer. Figure 4.7 illustrates the actual connection of the pieces of equipment to the module and the reference cell.

(a)   (b)
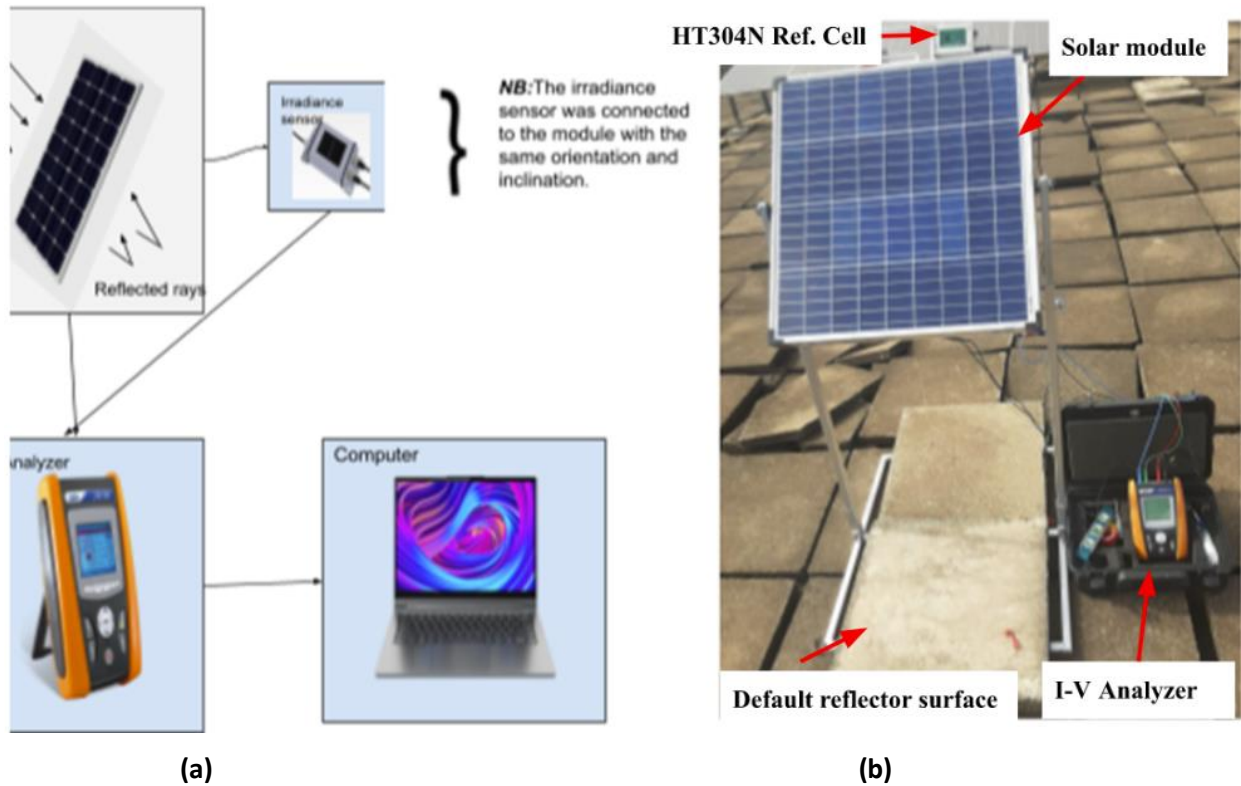
Figure 4.7. A layout of the equipment interconnection (a) and the actual experimental setup (b)

4.4: **Optimization of Ground Elevation**

To optimize the module's elevation from the ground, the module was kept horizontal (here defined as zero degrees). When collecting the I-V data at each elevation, the distance between the bottom side of the module and the ground level varied from 1.0 m to 1.5 m. The data were collected at an interval of 30 minutes from 10.00 am to 3.00 pm, EAT. This was repeated several times. The data was then analyzed to provide the most excellent ground elevation. Figure 4.8 shows the experimental setup for the module's elevation optimization at a zero-degree tilt angle.
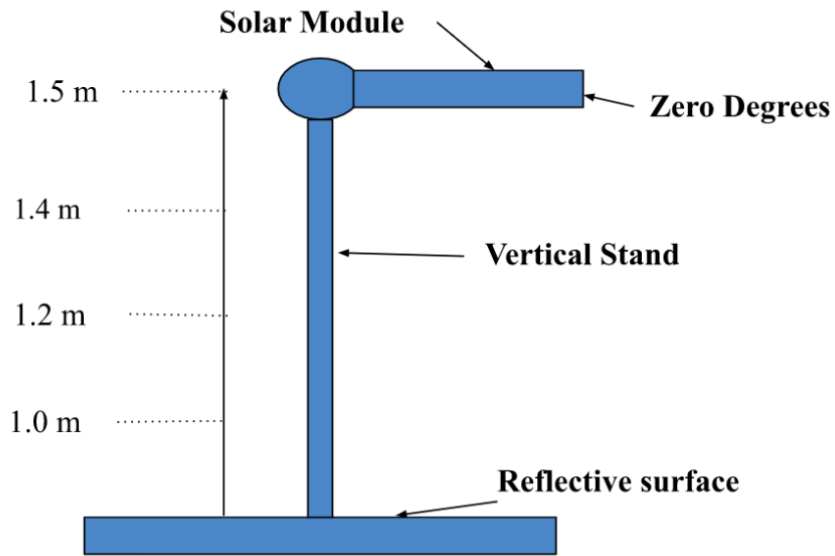
Figure 4.8: Setup for module elevation optimization with a zero-tilt angle

4.5: **Optimization of Tilt Angle**

The module's tilt angle was optimized by maintaining the ground elevation of the module at the optimal height obtained from section 4.4 while adjusting the tilt angle of the module from $0°$ up-to $90°$ at an increment of $30°$. Smaller angle increments was considered not to yield any significant difference in data. The I-V data at each tilt angle was then taken at intervals of 30 minutes between 10:00 am and 3:00 pm Eastern Standard Time (EAT). This procedure was repeated twice for each angle. Figure 4.9 shows how the module tilt angle was optimized at a fixed elevation of 1.2 m.
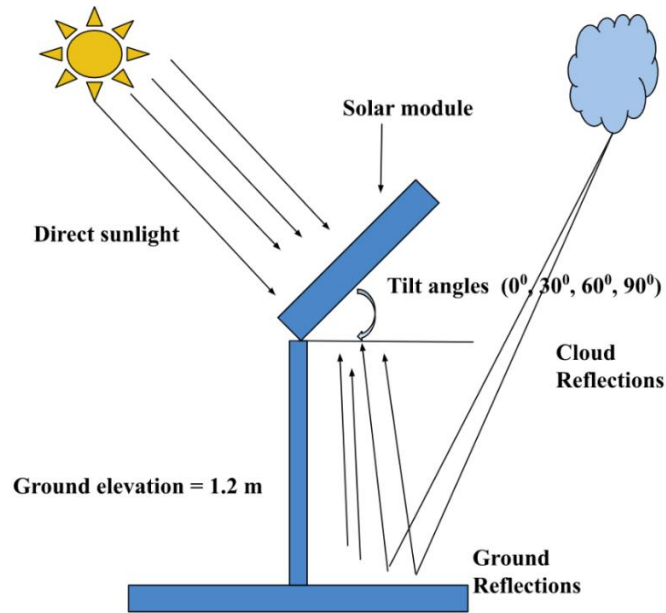
Figure 4.9: Tilt-angle optimization of the module at a fixed elevation of 1.2 m

4.6: **Effect of Reflective Surfaces**

This section explains how the impacts of reflecting surfaces on the performance of the bifacial module were explored when the reflective surfaces were put on the backside of the module. The module was installed at the optimized elevation obtained in section 4.4 and at the optimized tilt angle obtained in section 4.5. Three different surfaces (MPET material, a Mylar windshield sunshade, and a normal corrugated iron sheet) were placed under the module setup. The study was conducted a few minutes before noon and a few minutes after noon with no clouds and shading to get maximum solar irradiation. Data were collected at 2-minute intervals, and these data were recorded for each type of reflector. The data was analyzed, and the values for the three surfaces were compared to the values obtained for the default surface, concrete. Figure 4.9 shows a reflective surface setup with a tilt angle of 30° and an elevation of 1.2 meters.
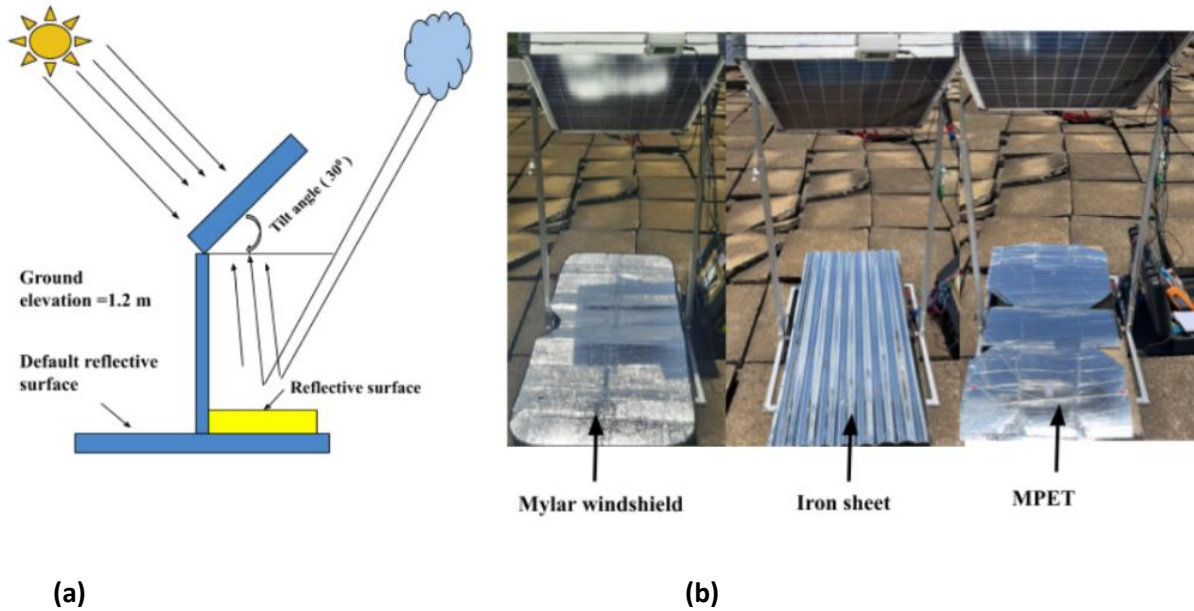
Figure 4.10: The design of the experimental setup (a) and the actual experimental arrangement (b) addressing the use of reflecting surfaces positioned below the backside of the module.

A simulation using PVGIS software for the same field of study was performed and validated using the measured data from the experiment. Using metrological data from the PVGIS software, the simulation was run at an angle of 30 °, which was the ideal angle for rooftop erections, and this was done when there was clear sky, diffuse irradiance, and direct sunlight during the 2 months and 15 days, i.e., in February and March 2022 when this study was conducted. The analysis was carried out utilizing factors that have a direct influence on the power generated by bifacial modules.

The effects of different reflecting surfaces on the irradiance generation of the bifacial module's rear side before and after the employment of a reflector were explored in several efforts (three rounds for each reflector). This was done between 12 pm and 1 pm East African Time at an optimized tilt angle of 30° and an optimized ground elevation of 1.2 m. A comparison of the three reflectors was then performed to determine which reflector produced the most power.

CHAPTER FIVE: RESULTS AND DISCUSSION

5.0: Introduction

Data obtained with subsequent discussion and analysis is presented here. The different parts discuss the optimization of ground elevation and tilt angle, the influence of solar irradiance, module temperature, and reflecting surfaces on the performance of a bifacial solar panel (referred to as a module). Sections 5.1 and 5.2 provide the manufacturers' technical specifications for the module and the results of optimizing both the module's elevation and tilt angle, respectively. The variation of solar irradiance with elevation and tilt angle is discussed in Section 5.3, while in Section 5.4, the relation between the performance of the module and the amount of solar irradiation is shown. In the latter part of this chapter, sections 5.5 and 5.6, respectively, we investigate the effect of module temperature on module performance as well as the effect of using various reflecting surfaces on module performance.

5.1: Module Specifications

The manufacturer's ratings under Standard Test Conditions (STC) are shown in the following table, together with the calculated values of the solar module for both the front and backside.

Table 5.1: *The manufacturer's ratings under Standard Test Conditions (STC), as well as the tested and computed values of the 60 W solar module at an elevation of 1.2 m and a tilt angle of 30°*

Module specification	STC (1000 W/m², 25 °C)	The module's front side (1060 W/m², 42 °C).	The module's backside (94 W/m², 38 °C).
Power output, ± 0.05, P_{max} (W)	60.00	53.87	4.64
Max. Current, ± 0.01, I_M (A)	3.21	3.63	0.35
Max voltage, ± 0.01 V_M (V)	18.00	14.84	13.27
Short circuit current, ± 0.01 I_{SC} (A)	3.41	3.76	0.37
Open circuit voltage, ± 0.01, V_{OC} (V)	22.20	20.48	17.48
Fill Factor, ± 0.01, FF	0.74	0.70	0.71
Module's Efficiency, ± 0.01%, η	14.88	14.65	14.01

The values that were calculated for the short-circuit current and the maximum current for the front side of the module were found to be greater than the ratings that were given by the manufacturers, an observation that was attributed to the higher irradiance experienced during measurements. Jumaat and Othman (2018), in their work on solar energy measurement, observed similar findings. However, the manufacturers' ratings had higher open circuit and maximum voltage values than the ones obtained in this work. Solar photovoltaic modules experience a voltage drop when subjected to high temperatures. Thus, the high temperature ($42\,^{\circ}$C) during measurement lowers the open circuit voltage, which explains why the measured voltage is lower than the manufacturer's ($17\,^{\circ}$C higher than the manufacturer's). Due to different operating conditions, the backside values were lower than the manufacturer's rated values. These results agreed with those that Durusoy and his colleagues had previously published (2020). The Fill factor and module efficiency were also computed. To calculate the fill factor (FF) and the module efficiency, equations (3.5) to (3.7) in Chapter 3 Section 3.4. were used.

Using maximum current and voltage measurements, the power output was calculated to be 53.87 W for the front and 4.64 W for the back, for a total of 58.51 W. In the absence of the backside (mono-facial case), the power output would be 53.87 W. Thus we have an additional power output due to the backside with an increase of 8.61%.

The front side of the module had a fill factor of 0.70, while the backside had a fill factor of 0.71; indicating more or less the same value. According to Table 5.2 below, the solar module used in this work was a high-quality solar module. This explains the close values of the fill factor. The results contrast the findings by Alquennah and Alasfour (2018) who obtained significantly different values for the front and backsides. Alquennah and Alasfour attributed the differences to variations in series and shunt resistance between the two sides.

Table 5.2: Classification of solar cell/module based on fill factor (Pujahari, 2021)

Classification	Values
Ideal FF	1
High quality	≥ 0.7-0.8
Low quality	< 0.7

The maximum efficiency obtained in this work was 14.65 ± 0.01% for the front side and 14.01 ± 0.01% for the backside. The efficiency disparity is caused by a mismatch in the irradiance received by each side (the front is exposed to direct solar irradiation, while the back is exposed to reflected and diffused irradiation creating higher internal resistance for the backside. Duran (2012), reported a similar trend. The efficiency values obtained in this work were within the range of those obtained by Bilčík *et al.*, (2020).

5.2: **Effect of Tilt Angle and Elevation on Module Performance**
5.2.1: **Effect of module Elevation**

Figure 5.1 depicts the results of a study that compared power production to elevation. Because of the high irradiance received on the front side, the values on the front side are typically higher than the values on the backside.
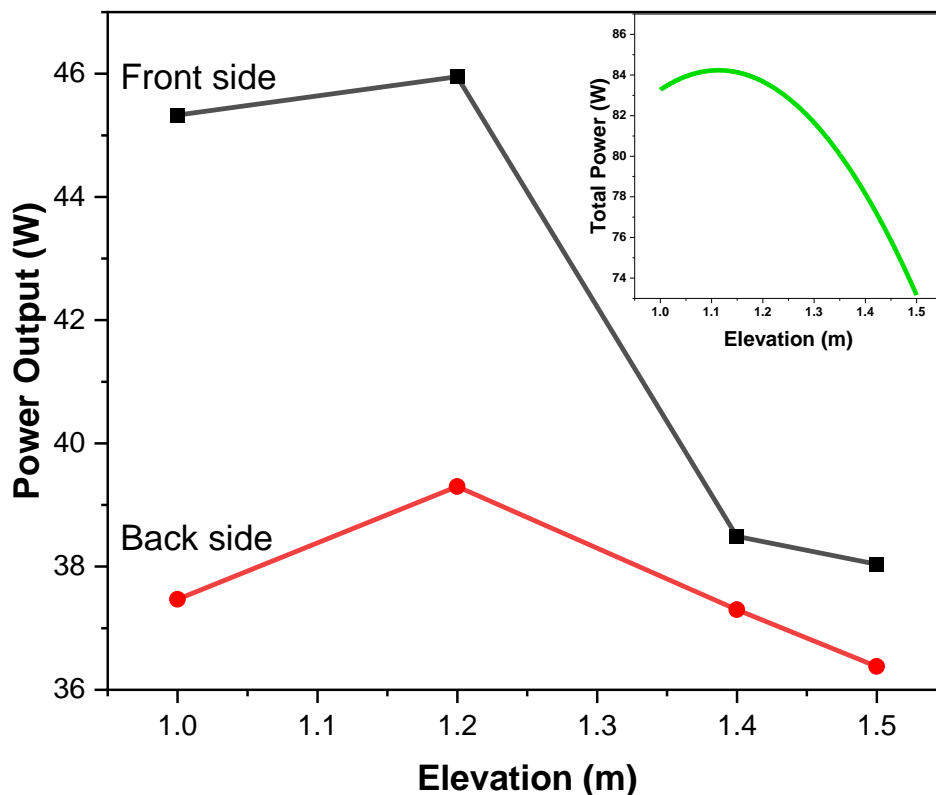
Figure 5.1: Variation in power output with elevation for the front and backsides (main graph) and the total power for both sides (inset) at a tilt angle of 30°at irradiation of 1016 W/m² and 97 W/m² respectively.

As seen in Figure 5.1, increasing the module's ground elevation increases the power output up to an elevation of about 1.2 m, and thereafter the power reduces. An elevation of 1.2 m was found to produce the most power output for both the front (45.95 W) and back (39. 30 W) of the module, so this elevation was chosen as the optimal elevation. A similar trend has been observed by other workers (Global, and Jinkosolar, 2021). This is a result of the module's elevation being raised to a higher level. decreases the amount of radiation that is reflected, which leads to a decrease in the amount of power produced.

5.2.2: **Effect Angle of Tilt**

Figure 5.2 shows how the tilt angle affects the amount of power that is produced at the optimized elevation of 1.2 m. It is crucial to note that the power output acquired from the module's front side was higher than that which was gained from the module's backside. This is due to the fact that the irradiance that strikes the front side module is greater than that which strikes the rear side module.
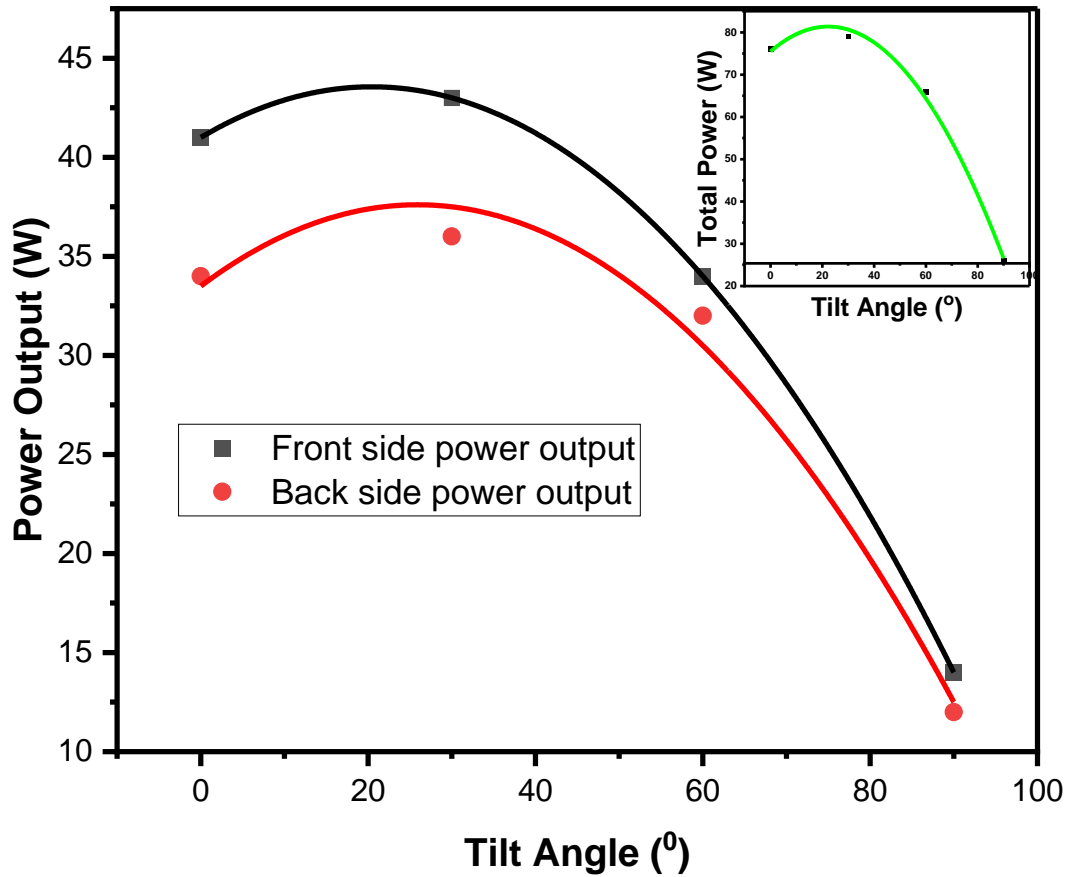
Figure 5.2: Variation of power output with tilt angle for the front and backside (main graph) and the total power output for both sides (inset) at an irradiance of 1016 W/m^2 and 97 W/m^2 respectively at an elevation of 1.2 m.

It was noted that as the angle of inclination increased, the power output increased slightly to a maximum of about 43 W (front side) and about 36 W (backside), then there was a steep decrease. The optimal tilt angle for both maximum power outputs was about 30º. As the angle of inclination increased beyond 30º, the module experienced less direct radiation from the sun hence the decrease in the power output. The optimum tilt angle was chosen as 30º. The findings on the tilt angle in this work are in concurrence with that of Dong *et al., (2009).*

5.3: **The variation of Solar Irradiance with Daylight Hours, Elevation, and Tilt Angle**

5.3.1: **Variation of solar irradiance with the time of the day**

Figures 5.3(a) and (b), depict how solar irradiance changed with time for both the front and backsides of the modules, from morning (10.00hrs) to afternoon (15.00hrs).
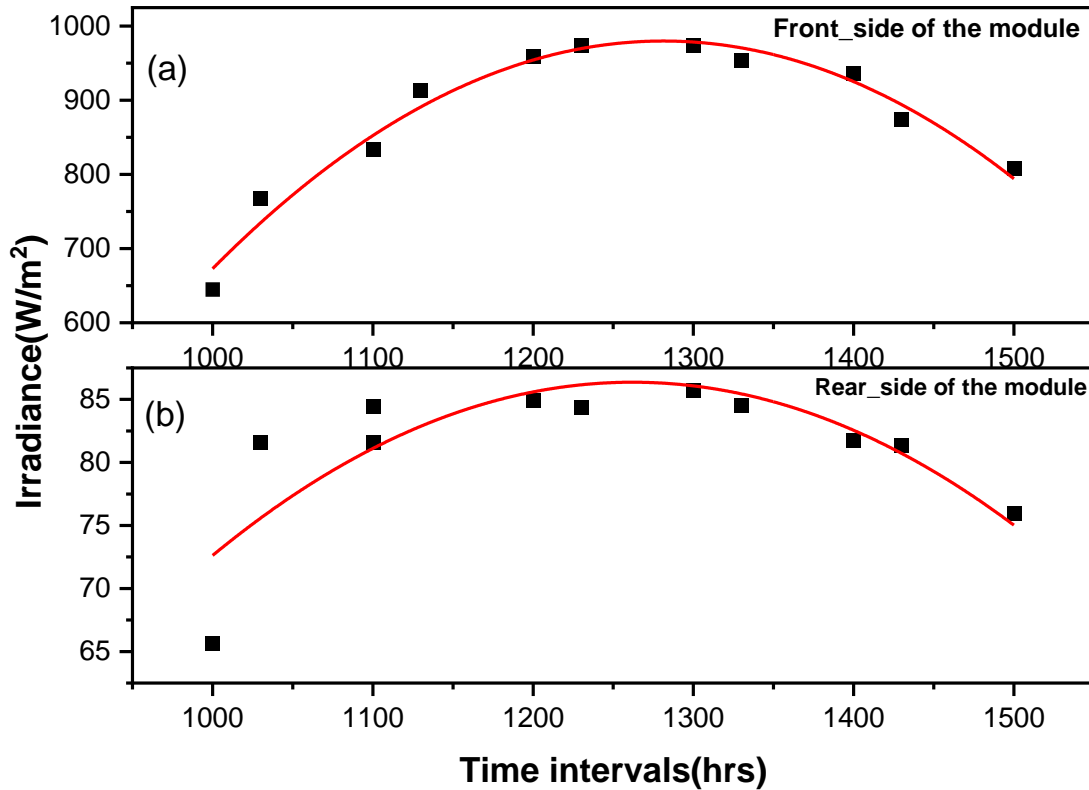
Figure 5.3: Variation of solar irradiance during the day on the front (a) and rear (b) sides of the module at the Chiromo Campus of the University of Nairobi (1.2732° S, 36.8049°) at a ground elevation of 1.2 m and a tilt angle of 30ᵒ

It was observed that there was a nearly normal distribution of the two plots, i.e., there was a rise in the morning hours, which peaks at noon and then fall in the afternoon. The rise from 10:00 to 12:30 may be ascribed to an increase in irradiance that is induced by the sun's radiation crossing a bigger radius while peaking at noon because of the least Sun-Earth distance, therefore the maximum irradiance. Comparable conclusions were found by Taylor and his companions in their investigation of the relationship between timeline and sun angles (Taylor *et al*., 2019). In other

words, the observed gradual decline in irradiance was attributed to the sun moving from a lower angle to a greater angle. It was further observed that the front side (a) received higher irradiance as compared to the backside (b) and this is because the front side captures direct sunlight whereas the backside receives reflected sunlight from both the albedo and surrounding of the solar module setup as explained by Durusoy and his colleagues (2020). The simulation done to validate this observation was found to have a normal distribution, which was consistent with the experimental work done in this work. This is shown in Figure 5.4, which depicts a graph of daily irradiance versus hours in Coordinated Universal Time (UTC + 3 = East African Time, EAT).
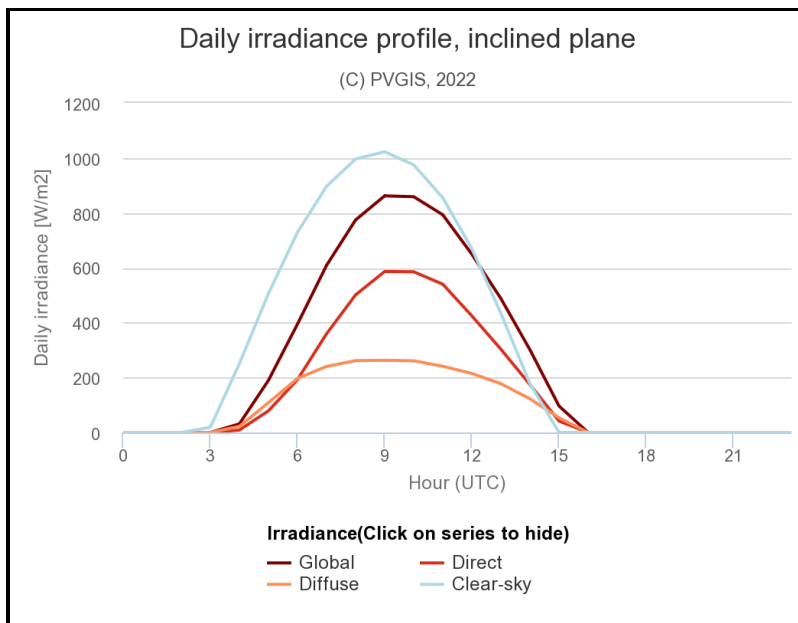
Figure 5.4: A simulation of the variation in daily average solar irradiance in February to March (2022) at a 30º inclined angle on the Chiromo Campus, University of Nairobi.

5.3.2: **The variation in solar irradiation with module adjustment in terms of elevation**

Figure 5.5 depicts the fluctuation in solar irradiance with the elevation of the module on both the front side (a) and the back side (b) of the module. It was noted that there was a general increase in solar radiation between the elevations of 1.0 m and 1.2 m for both sides of the module, which decreased further as the elevation increased to 1.5 m at a tilt angle of 0 degrees.
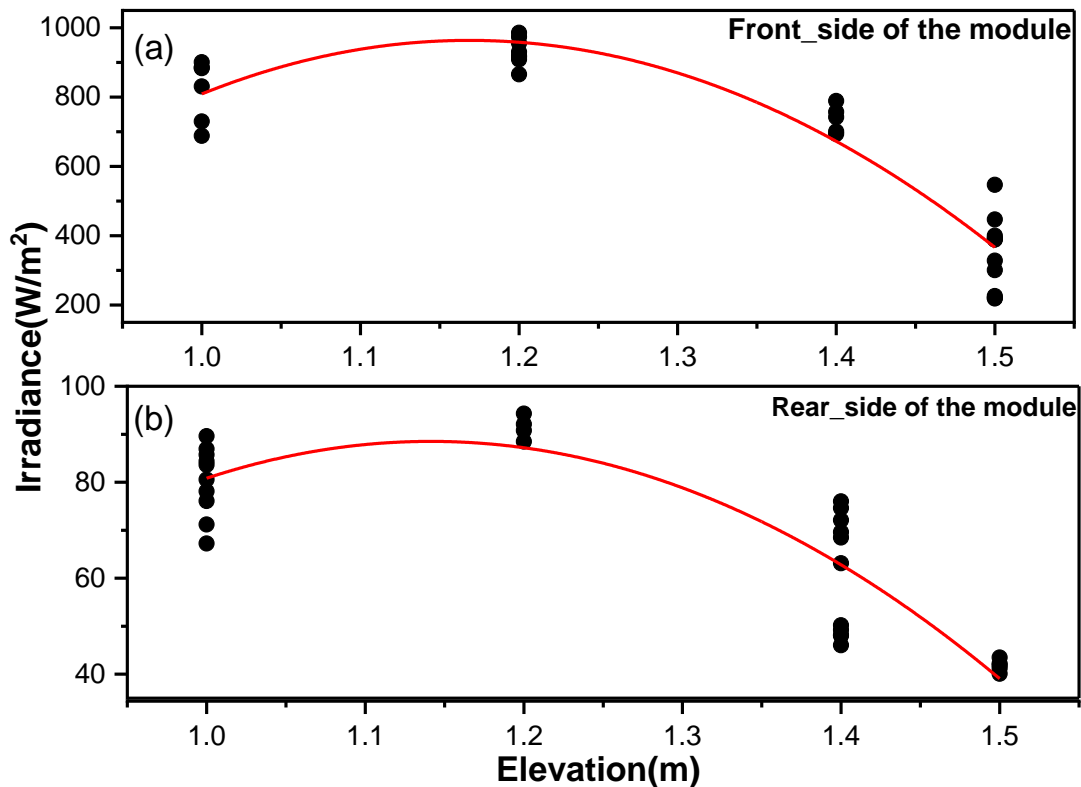
Figure 5.5: Variation of solar irradiation on the front (a) and back (b) sides of the module with elevation at set angle of 0°.

An increase in solar radiation can be attributed to an increase in global radiation as the elevation increases. Similar observations were found by (Blumthaler *et al*., 1997; Aldobhani, 2014). This behavior was seen for both the front side and the rear side of the module. At an elevation of 1.2 m, the front side of the module received a maximum irradiance of around 950 W/m^2, while the lowest irradiance was about 250 W/m^2 at 1.5 m elevation. The maximum solar irradiance was 93 W/m^2 at 1.2 m elevation and the lowest was 43 W/m^2 at 1.5 m for the module's backside. It was further observed that the front-side irradiances were greater than the back-side irradiances, which was because the front side of the module received direct sunlight, as opposed to the backside. It was also noted that beyond an elevation of 1.2 m for both sides of the module, the irradiance decreased. This result indicates that elevating a bifacial module beyond 1.2 m causes the backside of the module to receive insufficient irradiation, resulting in a reduction in power production. These

findings were consistent with those of Asgharzadeh et al. (2018), who investigated the effect of installation conditions on the efficiency of bifacial PV arrays.

5.3.3: **Relationship between solar irradiation and tilt angle**

Analyses were conducted to determine the connection between irradiance and tilt angle, and the findings are shown in Figure 5.6. It was noted that there was a general drop in solar radiation for both sides of the module as the tilt angle rose.
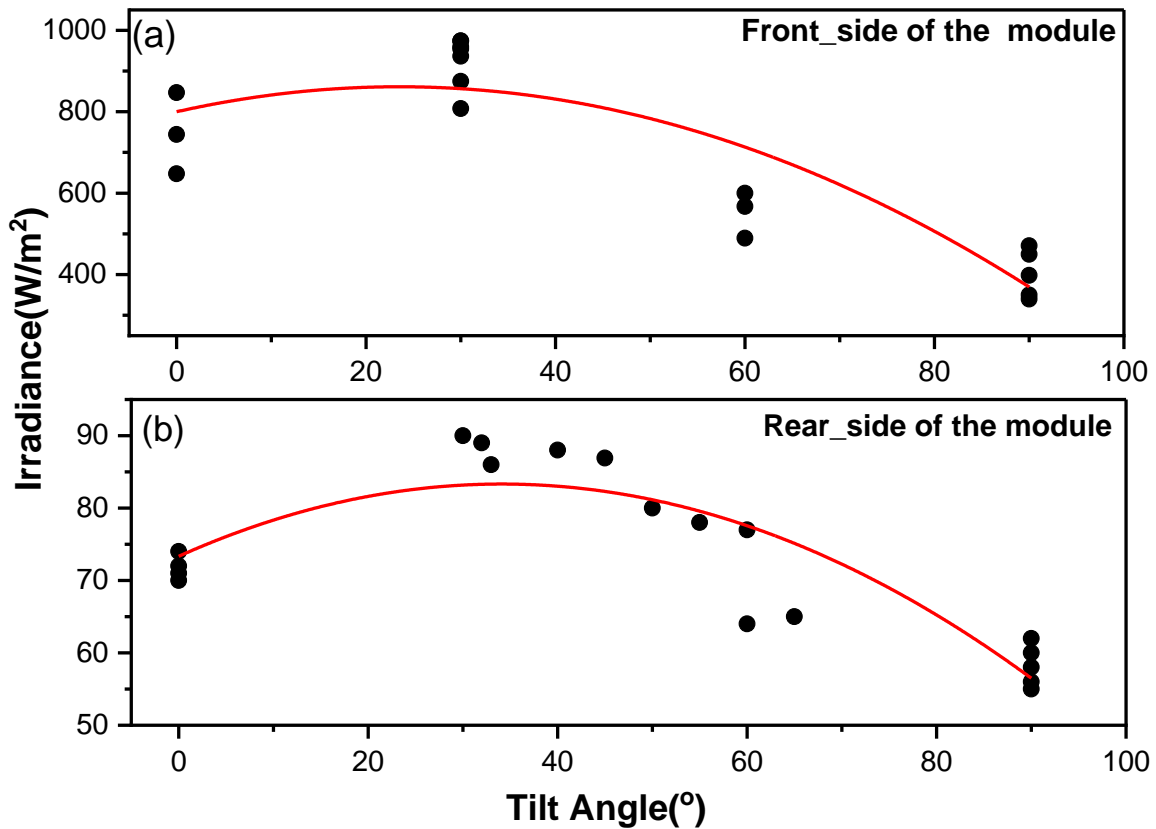
Figure 5.6: Variation in solar irradiation with tilt angle for the module's front (a) and back (b) sides.

As previously stated, the front-side values for irradiance were generally higher than the back-side values due to direct irradiance. Figure 5.6 above shows an increase in irradiance from 0° and peaking at about 30° and thereafter a steady decline in irradiance. This was observed for both sides of the module. The maximum irradiance observed for the front side was 970 W/m^2, (at a tilt angle of 30°) while the lowest irradiance was 110 W/m^2 at 90°. The maximum irradiance was 88 W/m^2

at 30º and the lowest irradiance was 62 W/m^2 at 90º for the module's backside. This work demonstrates that there is an optimum angle of tilt for modules. Sun and his colleagues observed similar results in their 2018 work on the optimization and performance of bifacial modules (Sun *et al.*, 2018)

5.4: **Influence of Solar Irradiance on the Overall Performance of the Bifacial Module**

This part discusses how the amount of solar irradiation influences the productivity of bifacial solar modules. It focuses primarily on the impacts that solar irradiation has on power production, short-circuits current, and maximum current, and it does so for both the front and the rear sides of the module.

5.4.1: **Effect of solar irradiation on short circuit and at maximum current**

Figure 5.7 (a-d) illustrates how the short-circuit current and maximum current change as a result of an increase or decrease in the amount of solar irradiation striking the front or rear of the module. Short-circuit current is proportional to the amount of solar irradiance that is received by the module, and it rises as the amount of solar irradiance increases. This is because the increased sunlight creates more current in the module. As solar irradiation rises, so does the module's maximum current. On both sides of the module, the maximum current and short-circuit current were observed to be directly related to solar irradiation. Similar results were found by Naamandadin et al, (2018).In conclusion, an increase in solar irradiance will generally increase in both of these parameters, although the exact relationship will depend on the specific characteristics of the module.
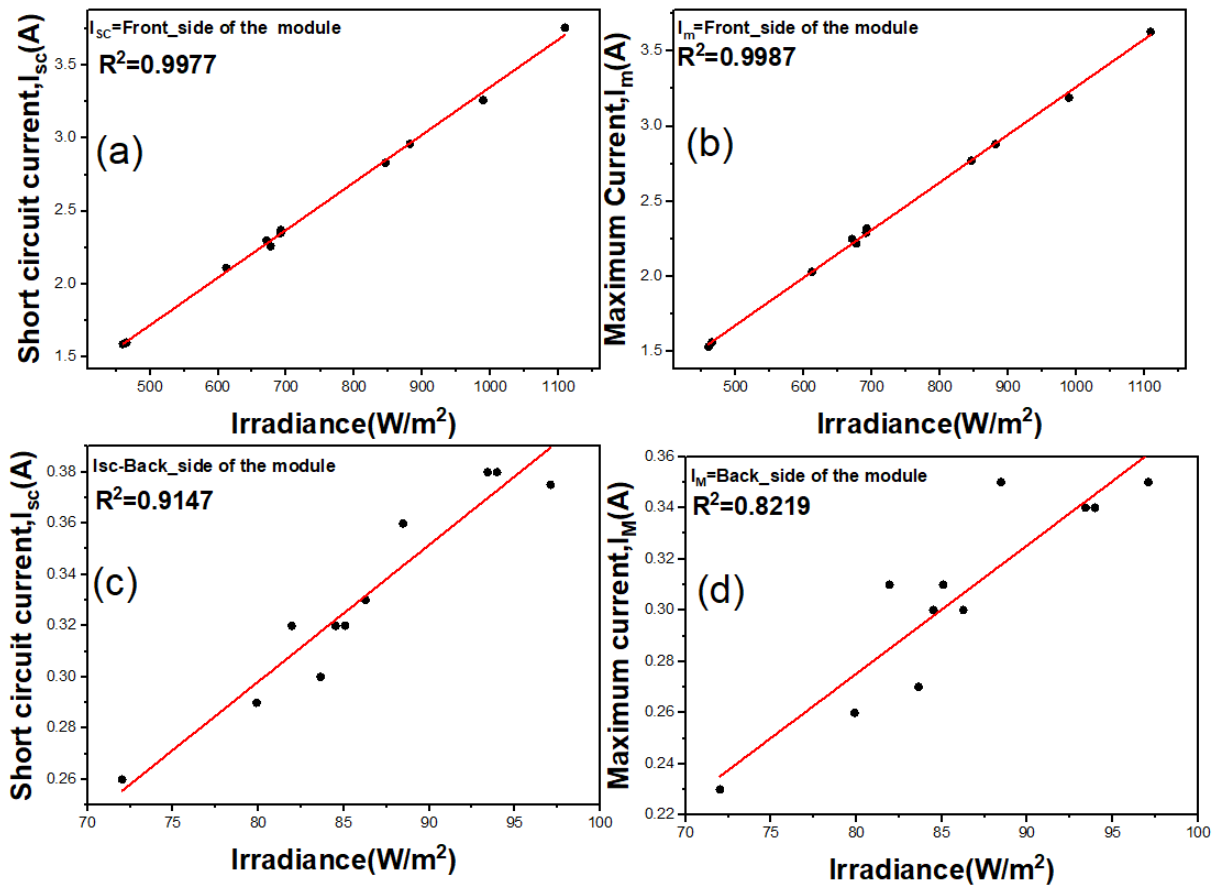
Figure 5.7: Plots showing how short circuit current and maximum current change with solar irradiation for the front (a,b) and back (c,d) sides of the module

The maximum current produced by the module's front side was 3.75 A at 1050 W/m^2, while the least current is 1.52 A at 405 W/m^2. The maximum current produced by the module's backside was 0.37 A at 97 W/m^2, while the lowest maximum current is 0.25A at 71 W/m^2. The R^2 values were over 0.99 for the front side indicating a very strong relationship between the solar irradiance and current. The values were, however, lower for the backside. The strong relationship between current and solar irradiance is explained by an increase in photoelectrons generated by the module's exposure to more solar irradiance. Similar findings were made found by Musanga *et al.*, (2018).

5.4.2: **Impact of solar irradiation on the amount of power generated**
Figure 5.8 (front side) and Figure 5.9 (back side) illustrate the findings of this study on the relationship between the amount of solar irradiation and the power generated. Both graphs show a direct proportionality relationship between power output and solar irradiance.
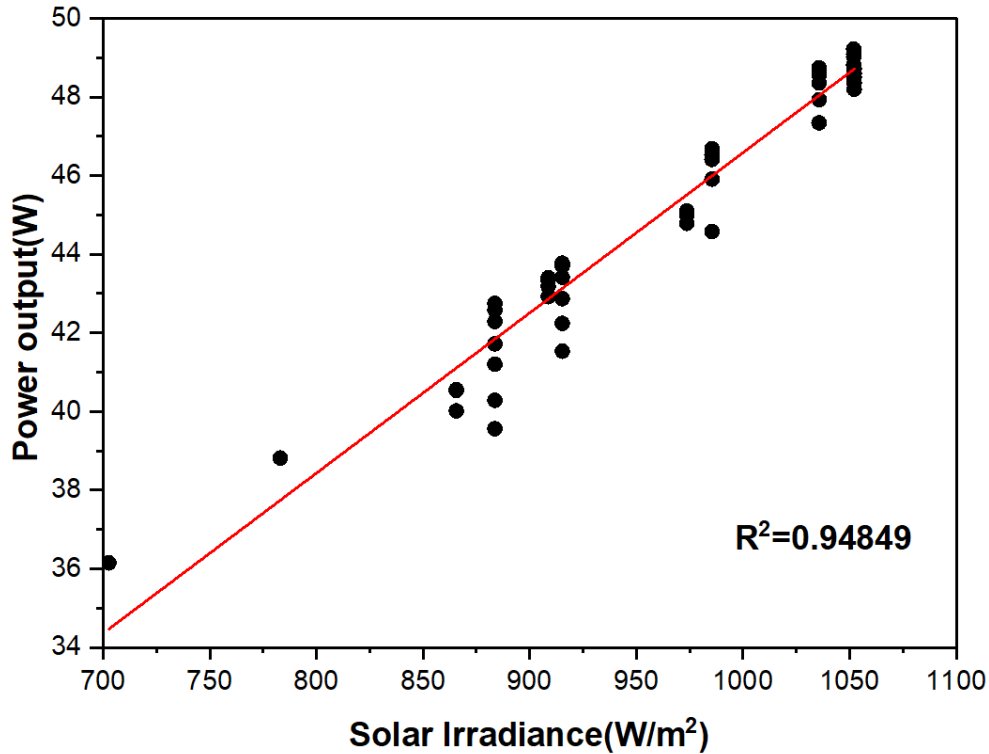
Figure 5.8: A graph of the front-side power output of the module versus solar irradiance

The greatest power output for the module's front side was 53.87 W at 1060 W/m^2 solar irradiance, while the lowest power output was 34.3 W at 718 W/m^2 solar irradiance. Maximum power production from the module's backside was 48.15 W at solar irradiation of 94.46 W/m^2, and minimum power output was 15.6 W at solar irradiance of 40 W/m^2. The linear fit demonstrates that power increases are directly proportional to solar irradiation, confirming the same trend as with current and irradiance discussed above. The strong correlation between power output and irradiance is evident from the high R^2 values of roughly 0.95 for the front side and 0.98 for the backside. This correlation can be explained by the fact that there was an increase in the rate of photon emission as the solar irradiance increased, which led to an increase in power output.
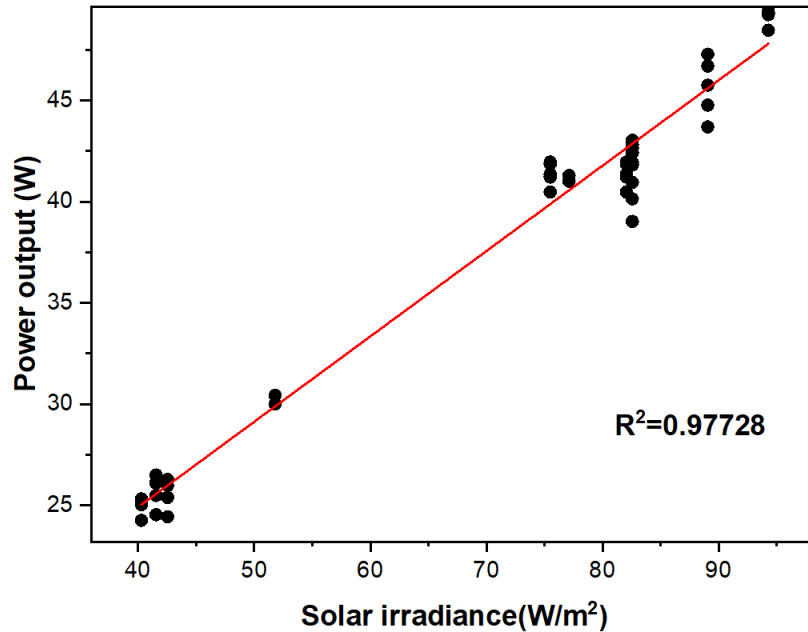
Figure 5.9: A graph of power output versus solar irradiance for the module's backside.

5.5: **The impacts that Module Temperature has on the Overall Performance of the Module**

The effect that module temperature has on the performance of the bifacial module is described in the following subsections. These subsections place an emphasis on how temperature affects the tilt angle of the module, the elevation of the module above the default ground, the maximum power output, and the open circuit voltage.

5.5.1: **Temperature of the module and its effect on the open circuit voltage**

Figure 5.10 illustrates how the temperature of the module affects the voltage across an open circuit. It was observed that as the module's temperature increased, there was a linear decrease in open circuit voltage. The strong negative correlation was supported by an R^2 value of about 0.96. This is due to an increase in the energy bound of the material's electrons as temperature rises, which interferes with the module's electrical parameters. The excited state of the electrons can thus be achieved more easily by reducing the open circuit voltage. These findings were in line with Dash's previous research on the impact of temperature on the performance of the PV module by (Dash and Gupta, 2015).
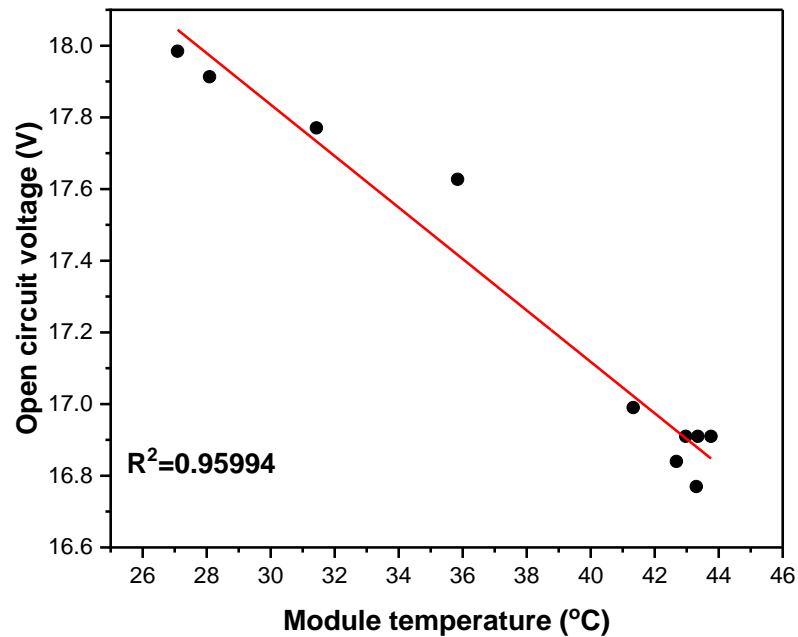
Figure 5.10: The module temperature variation with the open circuit voltage

5.5.2: **The impact that elevation above ground level has on the temperature of the module**

The relationship between the temperature of the module and the elevation above the ground is illustrated in Figure 5.11. As the elevation on each side of the module increased, the temperature of the module reduced. This is because elevating a solar module above the ground level increases airflow hence reducing its operating temperature which in turn improves its efficiency and power output. This demonstrates an inversely proportional relationship between module temperature and ground elevation with a strong correlation value of about 0.93. Comparable results were found by Dash and Gupta, (2015) by Xu *et al*., (2018) and Fouad *et al*., (2017). However, the exact relationship between module temperature and module elevation depends on factors such as local climate, shading patterns, and wind conditions which all impact the cooling of the module.
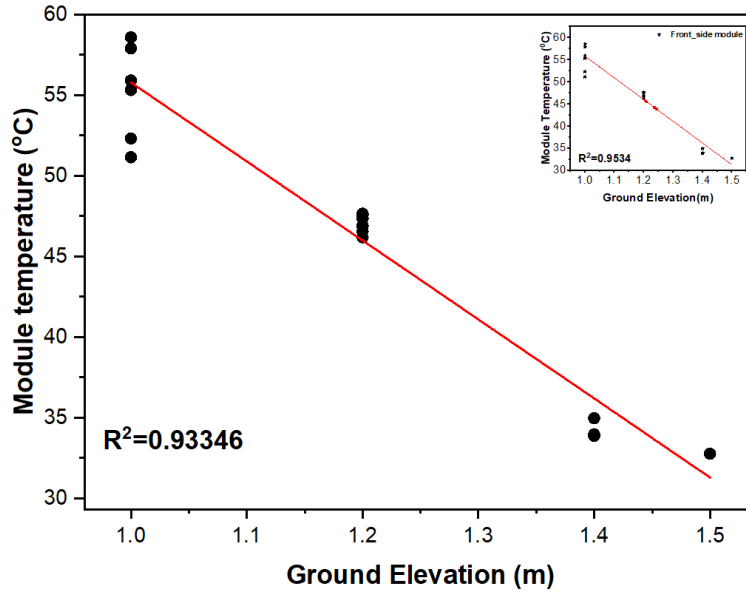
Figure 5.11: The module temperature fluctuations with ground elevation for both the backside (the main graph) and the front side of the module (inset)

5.5.3: **The impact of the angle of tilt on the temperature of the module**

The relationship between the temperature of the module and its tilt angle is illustrated in figure 5.12. It was observed that the module temperature dropped when there was a rise in the inclination angle. This is because as the angle of inclination is increased, the quantity of sunlight that can reach the module's surface area decreases. As a result, the temperature drops by a significant amount. The maximum module temperature was approximately 53.7° C at a tilt angle of 0° (front side) while the lowest temperature was roughly 31.3 $^{\circ}$C at an inclination angle of 90 $^{\circ}$. This demonstrates a strong relationship between the module temperature and the tilt angle, with an R^2 value of 0.94 for the backside and 0.97 for the front side. The relationship between these two variables agrees with Xu *et al.*, (2018); Ambarita *et a*l., (2018) findings. The findings mean that a balance has to be established for the right tilt angle that also gives maximum power since the module temperature drops with the increase of tilt angle.
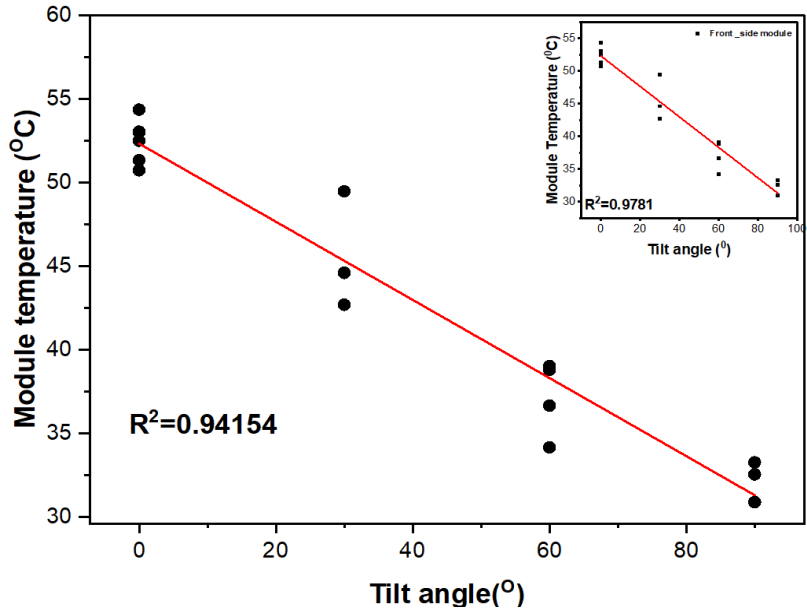
Figure 5.12: The module temperature fluctuations with ground elevation for both the backside (the main graph) and the front side of the module (inset)

5.6: **The Effect of Reflective Surfaces on the Module's Power Output**

Table 5.3 presents a comparison of the impact of a variety of reflecting surfaces on the irradiance generation of the rear side of the bifacial module both before and after the use of a reflector. In this case, attempts denote the number of times the various reflectors were placed beneath the module's backside.

Table 5.3: *Comparison of the effects of different reflective surfaces on the irradiance generation of the bifacial module's rear side before and after using a reflector.*

Type of reflector	Attempts	Solar Irradiance (W/m^2)		% increase, ±0.01
		Before the use of a reflector, ±0.01	After the use of a reflector, ±0.01	
Iron sheet	1	96.31	118.11	22.64
	2	106.10	129.63	22.18
	3	91.44	113.43	24.05
Mylar sunshade	1	110.35	194.39	76.16
	2	110.47	190.41	72.36
	3	107.31	196.50	83.11
MPET	1	111.43	200.01	79.49
	2	109.05	203.14	86.28
	3	108.39	205.22	88.19

According to Table 5.3, it is clear that the amount of solar irradiation on the backside before the use of reflectors was lower than after the use of reflectors. This observation was attributed to the rear side's low irradiance, which is primarily from diffused and reflected irradiances. The high values observed from the MPET reflector are due to the high reflectivity material used in the fabrication of this type of reflector. For the iron sheet, Mylar sunshade, and MPET, the average irradiance increase was 22.95%, 77.21%, and 84.62 %, respectively.

The amounts of irradiance produced with and without reflective surfaces are depicted in Figures 5.13 - 5.15. In general, there was low irradiance before the use of the reflector for all three surfaces. In the same way that low irradiance from reflected and diffused irradiances accounted for the poor performance of the module's backside, so too can this phenomenon be explained. It was also found that regardless of the reflective surface used, there was a general increase in irradiance, which was because the back of the module was exposed to a greater quantity of light thanks to the use of reflectors. It was also further observed that out of the three reflector samples used, the MPET reflector produced the most irradiance, followed by the Mylar sunshade reflector, and finally the

galvanized iron sheet reflector. The various attempts confirmed the consistency of each reflector used, as well as whether it was significantly increasing the irradiance.
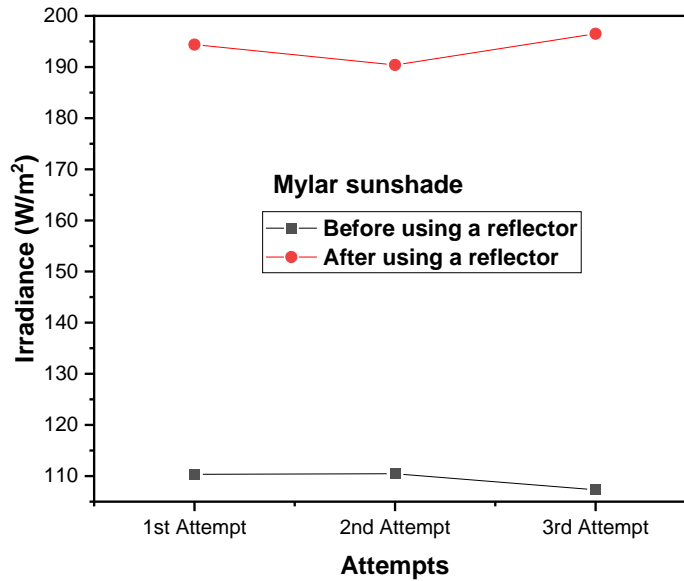
Figure 5.13: A graph of irradiance versus the number of attempts with and without a Mylar windshield sunshade reflector.
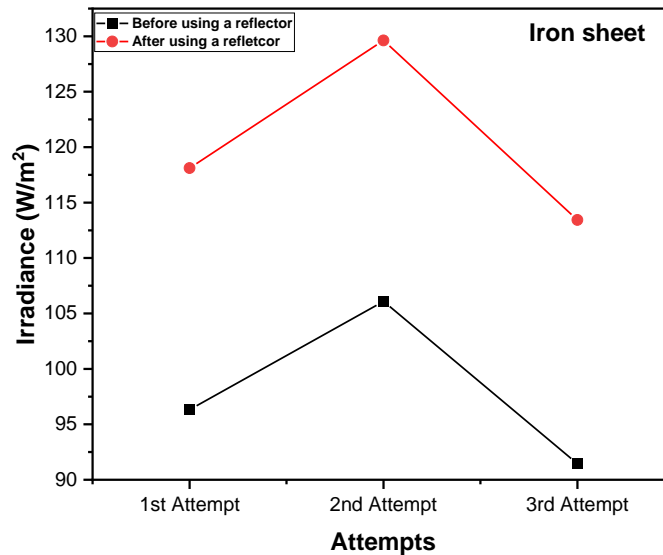
Figure 5.14: A plot of irradiance versus the number of attempts with and without a Mylar iron sheet reflector.
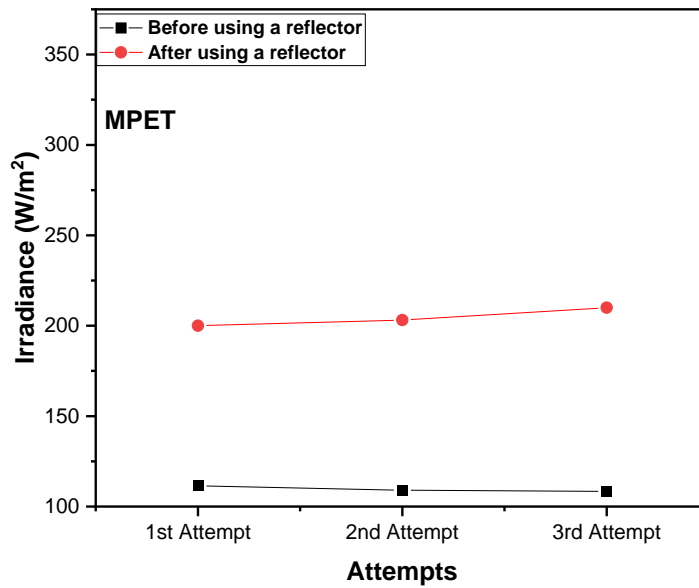
Figure 5.15: A plot of irradiance versus the number of attempts for the module's backside with and without the use of an MPET reflector

Figure 5.16 compares the three reflectors used in this study in terms of irradiance increase with the number of attempts
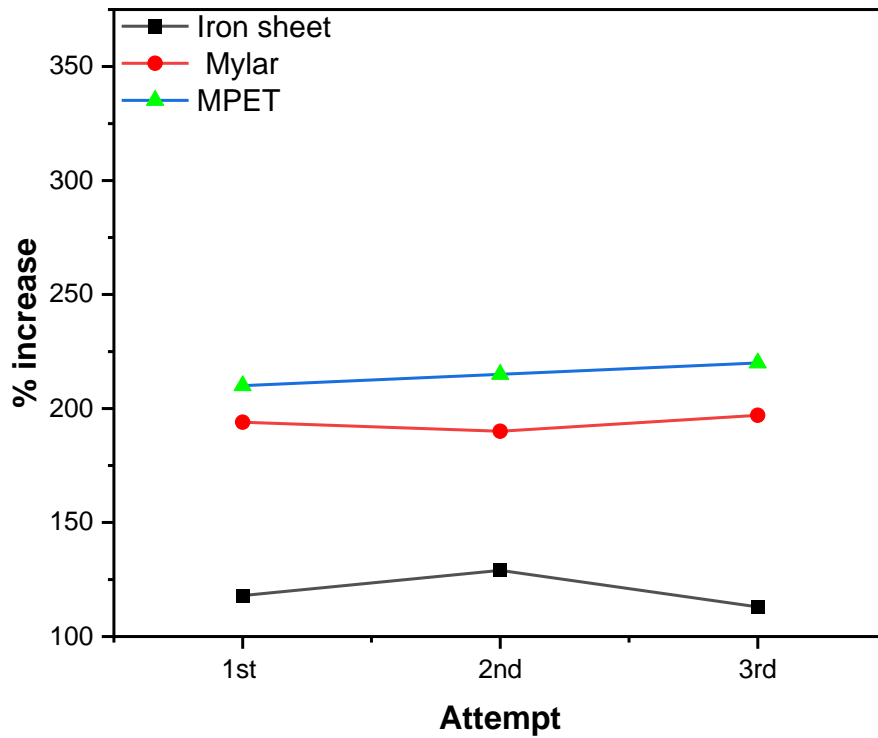
Figure 5.16: A plot of the percentage increase in irradiance versus the number of attempts made for various reflectors when placed beneath the module's backside

As per figure 5.16, the highest impact was made by metalized polyethylene terephthalate (MPET), followed by Mylar, and finally by galvanized iron sheet, as previously stated. According to the findings of this study, the MPET is highly recommended for use as a backside module reflector, because of its high reflectivity.

Table 5.4 shows the power produced before and after using the reflective surfaces.

Table 5.4: *A comparison of the effects of various reflective surfaces on bifacial module power generation*

Background ⟋ Performance	Concrete-default surface, ±0.0 1, (W)	MPET Reflector, ±0.01, (W)	Mylar windshield reflector, ± 0.01 (W)	Galvanized iron sheet reflector, ± 0.01, (W)
Power output, ± 0.01, (W)	57.43	65.32	60.40	58.50
% Increase	-	13.74	5.17	1.86

The amount of light reflected on the module's surface had a direct correlation to the amount of power that was generated by the module's back side. Additionally, it was observed that putting reflectors on the module's backside increased the amount of power that is produced. This observation is consistent with Martin and Tamizhmani's (2019) work, which produced comparable results. Cha *et al.,* (2018) found that using reflectors increases power output by more than 2% in their theoretical work on power prediction with different reflection conditions for bifacial modules, which is consistent with the findings from this study, where the least amount of power increase was 1.86% and the highest contribution was 13.74%. Because of the high reflectivity material used in making this type of reflector, the MPET reflector (which has been used in solar cookers due to its high reflectivity) contributed the most to the power output.

According to the findings of this research, it is possible to conclude that in an equatorial region like Kenya, where the sun spends most of the year at a high altitude in the sky, a steeper tilt angle may be used to optimize the amount of sunlight captured by the bifacial modules, further increasing their efficiency. It can also be concluded that the exact impact of elevation and tilt angle on the bifacial solar module will depend on factors such as specific location and shading patterns in the area which may need to be carefully considered in a study.

CHAPTER SIX: CONCLUSIONS AND RECOMMENDATIONS

6.0: Conclusions

The optimal elevation and tilt angle for placing a bifacial module, as well as the impact of background reflective surfaces in the tropics, have been the subject of this study. The obtained data were analyzed using Python and Origin software. The results revealed that: -

1. There was a general increase in solar irradiance as elevation increased from 1.0 m with an irradiance of (718.00 W/m^2) to a maximum of 1.2 m with an irradiance of 1060.00 W/m^2 for the front side and from 43.00 W/m^2 to 94.00 W/m^2 for the backside. Beyond 1.2 m, solar radiation gradually decreased as the module elevation was increased to 1.5 m; producing 250.00 W/m^2 for the front side and 43.00 W/m^2 for the backside.

2. There was a directly proportional relationship between power output and solar irradiance for the bifacial module. This meant that as the amount of solar irradiance increased/decreased, so did their output power. The maximum amount of power that could be extracted from the module's front was 53.87 W. at 1060 W/m^2 solar irradiance while the lowest power output was 34.30 W at 718.00 W/m^2 solar irradiance. The highest power output for the module's backside was 4.82 W at 94.00 W/m^2 solar irradiance. An elevation of 1.2 m produced the highest power output for both the front (53.8787 W) and back (48.15 W).

3. It was also concluded that the amount of sunlight reflected on both sides of the module decreased as the tilt angle increased. For the front side, the maximum irradiance that was measured was 1060 W/m^2 when the angle of inclination was 30º, and the minimum irradiance that was measured was 110.00 W/m^2 when the angle of inclination was 90º. The maximum irradiance was 96 W/m^2 at 30º and the lowest irradiance was 62.00 W/m^2 at 90º for the module's backside. The optimum angle of inclination for the module was determined to be 30º since it produced the highest power output values for both sides of the module; 43.00 W and 36.00 W for the front side and backside respectively.

4. The short-circuit current and maximum current were found to increase as solar irradiance increased, with R^2 of about 0.97 for the front side of the module and about 0.92 for the backside. Furthermore, it was observed that the Voc decreased as the temperature of the module increased; R^2 of around 0.96 confirms this observation. The default surface in this

work was concrete, and the three reflective surfaces were MPET, Mylar windshield shade structure, and galvanized iron sheet.

5. The results showed that the materials used to make the reflectors had varying reflective contributions, with some having higher reflectivity than others. MPET had the highest reflectivity out of the three reflectors, followed by Mylar and iron sheet.

6. It was also observed that the use of reflectors on the module's rear side increased the quantity of radiation received from the back of the module, with some reflectors contributing more irradiance than others. MPET produced the most irradiance of the three reflector samples tested, followed by Mylar sunshade and finally iron sheet. The irradiance increases percentages for MPET, Mylar, and iron sheets were 84.62 %, 77.21 %, and 22.95 %, respectively.

7. When reflectors were used, the module's power output was proportional to the amount of irradiance contributed by each reflector. The results revealed that the MPET reflector produced the most power, with a power production increase of approximately 13.74%, followed by the Mylar sunshade reflector at about 5.17%, and finally the galvanized iron sheet reflector contributing approximately 1.86%. The high reflectivity of MPET demonstrated in this work is due to the material used during fabrication, which is made of high reflectivity, and as a result, it has previously been used in the fabrication of solar cookers. Thus, this material is recommended for use as a reflector to complement the power output of the underside of the bifacial module, and by extension, the total power output of the module as a whole.

6.1: Recommendations for Further Work

Based on the research conducted in this work, bifacial technology appears to be a very promising option in the solar sector; however, more research is required;

1. To determine whether this technology can benefit solar home systems as well.
2. To study the effect of shading on bifacial module when integrated with other technologies
3. To investigate the cost effectiveness of bifacial modules

REFERENCES

Ademola, S., & Qiu, Y. (2020). *Potential of Bifacial PV Installation and Optimization*. *11*(12), 558–565.

Aldobhani, A. M. S. (2014). Effect of Altitude and Tilt Angle on Solar Radiation in Tropical Regions. *Journal of Sciency & Technology*, *19*(1), 96–109.

Ambarita, H., Siregar, R. E. T., Ronowikarto, A. D., & Setyawan, E. Y. (2018). Effects of the inclination angle on the performance of flat plate solar collector. *Journal of Physics: Conference Series*, *978*(1). https://doi.org/10.1088/1742-6596/978/1/012097

Arnoux, G., Bassi, N., Fakhfouri, V., Ambigapathy, R., Levrat, J., Despeisse, M., & Ballif, C. (2018). Toward the standardisation of the power rating of bifacial solar devices. *Meyer Burger*, 1–20.

Bilčík, M., Božiková, M., Kotoulek, P., Kišev, M., Csillag, J., & Petrović, A. (2020). Comparison of the annual power balance of photovoltaic modules. *Journal on Processing and Energy in Agriculture*, *24*(1), 18–21. https://doi.org/10.5937/jpea24-25659

Blumthaler, M., Ambach, W., & Ellinger, R. (1997). Increase in solar UV radiation with altitude. *Journal of Photochemistry and Photobiology B: Biology*, *39*(2), 130–134. https://doi.org/10.1016/S1011-1344(96)00018-8

Cha, H. L., Bhang, B. G., Park, S. Y., Choi, J. H., & Ahn, H. K. (2018). Power prediction of bifacial Si PV module with different reflection conditions on rooftop. *Applied Sciences (Switzerland)*, *8*(10). https://doi.org/10.3390/app8101752

Chen, Z., Chen, Y., Wu, L., Cheng, S., Lin, P., & You, L. (2019). Accurate modeling of photovoltaic modules using a 1-D deep residual network based on I-V characteristics. *Energy Conversion and Management*, *186*(December 2018), 168–187. https://doi.org/10.1016/j.enconman.2019.02.032

Cousse, J. (2021). Still in love with solar energy? Installation size, affect, and the social acceptance of renewable energy technologies. *Renewable and Sustainable Energy Reviews*, *145*(April), 111107. https://doi.org/10.1016/j.rser.2021.111107

Cubas, J., Pindado, S., & De Manuel, C. (2014). Explicit expressions for solar panel equivalent circuit parameters based on analytical formulation and the lambert W-function. *Energies*, *7*(7), 4098–4115. https://doi.org/10.3390/en7074098

Dash, P. K., & Gupta, N. C. (2015). Effect of Temperature on Power Output from Different Commercially available Photovoltaic Modules. *Journal of Engineering Research and Applications Www.Ijera.Com*, *5*(1).

Durusoy, B. (2020). *Description and Verification of a Model To Calculate the Efficiency of a Bifacial Pv Module Using Theoretical and Experimental Observations a Thesis Submitted To the Graduate School of Natural and Applied Sciences of Middle East Technical University*.

Durusoy, B., Ozden, T., & Akinoglu, B. G. (2020). Solar irradiation on the rear surface of bifacial solar modules: a modeling approach. *Scientific Reports*, *10*(1), 1–10. https://doi.org/10.1038/s41598-020-70235-3

Foldvik, O. (2019). *Investigation of Photovoltaic Energy Yield on Tromsøya by Mapping Solar Potential in ArcGIS. July*.

Goss, R. M. (1983). *BP statistical review of world energy 1982. June*.

Gu, W., Ma, T., Ahmed, S., Zhang, Y., & Peng, J. (2020). A comprehensive review and outlook of bifacial photovoltaic (bPV) technology. *Energy Conversion and Management*, *223*(August). https://doi.org/10.1016/j.enconman.2020.113283

Guerrero-Lemus, R., Vega, R., Kim, T., Kimm, A., & Shephard, L. E. (2016). Bifacial solar photovoltaics - A technology review. *Renewable and Sustainable Energy Reviews*, *60*, 1533–1549. https://doi.org/10.1016/j.rser.2016.03.041

Guerrero-Perez, J., Berbel, J. N., Muñoz Benavente, I., Navarro Berbel, J., Berbel, J. N., Singh, J. P., Aberle, A. G., Walsh, T. M., Rodríguez-Gallegos, C. D., Liu, H., Gandhi, O., Singh, J. P., Krishnamurthy, V., Kumar, A., Stein, J. S., Wang, S., Li, L., Reindl, T., Peters, I. M., … Heckmann, M. (2018). Optimal Mounting Configuration for Bifacial Solar Modules on Single Axis Trackers. *Soltec Whitepaper*, *176*(2015), 136–142.

Guo, S., Walsh, T. M., & Peters, M. (2013). Vertically mounted bifacial photovoltaic modules: A

global analysis. *Energy*, *61*, 447–454. https://doi.org/10.1016/j.energy.2013.08.040

Hasegawa, Y. (n.d.). *Planet Formation in Star-Forming Regions We can see planet- forming regions*.

I-V400w – SOLAR I-Ww I-V500w – SOLAR I-Ve. (2017).

Isabella, O., Smets, A. H. M., & Zeman, M. (2014). Thin-film silicon-based quadruple junction solar cells approaching 20% conversion efficiency. *Solar Energy Materials and Solar Cells*, *129*, 82–89. https://doi.org/10.1016/j.solmat.2014.03.021

Jao, M. H., Liao, H. C., & Su, W. F. (2016). Achieving a high fill factor for organic solar cells. *Journal of Materials Chemistry A*, *4*(16), 5784–5801. https://doi.org/10.1039/c6ta00126b

Kang, J. G., Kim, J. H., & Kim, J. T. (2016). Design elements and electrical performance of a bifacial BIPV module. *International Journal of Photoenergy*, *2016*. https://doi.org/10.1155/2016/6943936

Khan, M. R., & Alam, M. A. (2015). Thermodynamic limit of bifacial double-junction tandem solar cells. *Applied Physics Letters*, *107*(22). https://doi.org/10.1063/1.4936341

Liang, T. S., Pravettoni, M., Deline, C., Stein, J. S., Kopecek, R., Singh, J. P., Luo, W., Wang, Y., Aberle, A. G., & Khoo, Y. S. (2019). A review of crystalline silicon bifacial photovoltaic performance characterisation and simulation. *Energy and Environmental Science*, *12*(1), 116–148. https://doi.org/10.1039/c8ee02184h

Libal, J., & Kopecek, R. (2018). Bifacial photovoltaics: Technology, applications and economics. In *Bifacial Photovoltaics: Technology, applications and economics*. https://doi.org/10.1049/PBPO107E

Lo, C. K., Lim, Y. S., & Kee, S. Y. (2013). Improvement of bifacial solar panel efficiency using passive concentrator and reflector system. *Proceedings of 2013 International Conference on Renewable Energy Research and Applications, ICRERA 2013*, *October*, 42–45. https://doi.org/10.1109/ICRERA.2013.6749723

Lopez-Garcia, J., Casado, A., & Sample, T. (2019). Electrical performance of bifacial silicon PV modules under different indoor mounting configurations affecting the rear reflected

irradiance. *Solar Energy*, *177*(October 2018), 471–482. https://doi.org/10.1016/j.solener.2018.11.051

Louw, J., & Rix, A. J. (2020). *Modelling and simulation of bifacial PV modules by implementing the ray tracing technique*. *March*.

Luque, A. (1981). Theoretical bases of photovoltaic concentrators for extended light sources. *Solar Cells*, *3*(4), 355–368. https://doi.org/10.1016/0379-6787(81)90026-0

Luta, D. N. (2019). *An energy management system for a hybrid reversible fuel cell/supercapacitor in a 100% renewable power system*. *July*.

Maka, A. O. M., & Alabid, J. M. (2022). Solar energy technology and its roles in sustainable development. *Clean Energy*, *6*(3), 476–483. https://doi.org/10.1093/ce/zkac023

Musanga, L. M., Barasa, W. H., & Maxwell, M. (2018). The Effect of Irradiance and Temperature on the Performance of Monocrystalline Silicon Solar Module in Kakamega. *Physical Science International Journal*, *19*(4), 1–9. https://doi.org/10.9734/psij/2018/44862

Mwarabu, A. (2020). *Effect of purified natural dyes on dye-sensitized solar cell performance*.

Naamandadin, N. A., Ming, C. J., & Azani Mustafa, W. A. (2018). Relationship between Solar Irradiance and Power Generated by Photovoltaic Panel: Case Study at UniCITI Alam Campus. *Journal of Advanced Research in Engineering Knowledge*, *5*(January 2019), 16–20.

Njagi Nguu, J. (2017). *UNIVERSITY OF NAIROBI DEPARTMENT OF PHYSICS Fabrication and Characterization of TiO2/Nb2O5 Composite Photo-Electrodes Deposited Using Electrophoretic Technique for Application in Dye-Sensitized Solar Cells*.

Nussbaumer, H., Janssen, G., Berrian, D., Wittmer, B., Klenk, M., Baumann, T., Baumgartner, F., Morf, M., Burgers, A., Libal, J., & Mermoud, A. (2020). Accuracy of simulated data for bifacial systems with varying tilt angles and share of diffuse radiation. *Solar Energy*, *197*, 6–21. https://doi.org/10.1016/j.solener.2019.12.071

Okomoli, J. B. (2019). University of NAIROBI Library. *Tax Foundation*, *20*(7), 98–105.

Oliveti, G., Marletta, L., Arcuri, N., De Simone, M., Bruno, R., & Evola, G. (2014). Solar

energy. *Green Energy and Technology*, *0*(9783319030739), 159–214. https://doi.org/10.1007/978-3-319-03074-6_4

P.Baliozian, S.Tepner, M. F. (2020). The International Technology Roadmap for. *37th European Photovoltaic Solar Energy Conference (EUPVSEC)*, *September*, 7–11.

Pujahari, R. M. (2021). Crystalline silicon solar cells. In *Energy Materials: Fundamentals to Applications*. https://doi.org/10.1016/B978-0-12-823710-6.00004-2

Riedel-Lyngskær, N., Poulsen, P. B., Jakobsen, M. L., Nørgaard, P., & Vedde, J. (2020). Value of bifacial photovoltaics used with highly reflective ground materials on single-axis trackers and fixed-tilt systems: A danish case study. *IET Renewable Power Generation*, *14*(19), 3946–3953. https://doi.org/10.1049/iet-rpg.2020.0580

Rueter, M., Dobosz, M., & Wilk, R. D. (2021). A Study of Reflector-Enhanced Bifacial PV. *American Solar Energy Society National Solar Conference 2021 Proceedings, SOLAR 2021*, *2018*, 103–114. https://doi.org/10.18086/solar.2021.01.05

Salloom, A., Abdulrazzaq, O., & Ismail, B. (2018). Assessment of the Performance of Bifacial Solar Panels. *International Journal of Engineering and Technical Research*, *8*(7), 13–17.

Sharma, A., Kumar, S., & Editors, K. (2015). Green Energy and Technology Energy Sustainability Through Green Energy. In *Springer*.

Solar, J. (n.d.). *Swan Bifacial Modules*.

Stefan w., P. (2021). *Publishable Summary for 16ENG02 PV-Enerate Advanced PV Energy Rating*. *May*, 1–8.

Sun, X., Khan, M. R., Deline, C., & Alam, M. A. (2018). Optimization and performance of bifacial solar modules: A global perspective. *Applied Energy*, *212*(September), 1601–1610. https://doi.org/10.1016/j.apenergy.2017.12.041

Taylor, O. R., Lovett, J. P., Gibo, D. L., Weiser, E. L., Thogmartin, W. E., Semmens, D. J., Diffendorfer, J. E., Pleasants, J. M., Pecoraro, S. D., & Grundel, R. (2019). Is the Timing, Pace, and Success of the Monarch Migration Associated With Sun Angle? *Frontiers in Ecology and Evolution*, *7*. https://doi.org/10.3389/fevo.2019.00442

Wenham, S. R., Green, M. A., Watt, M. E., Corkish, R., & Sproul, A. (2017). *Stuart R. Wenham, Martin A. Green, Muriel E. Watt, Richard Corkish and Alistair Sproul*.

Xu, Z., Zhang, Y., Li, B., Wang, C. C., & Li, Y. (2018). The influences of the inclination angle and evaporator wettability on the heat performance of a thermosyphon by simulation and experiment. *International Journal of Heat and Mass Transfer*, *116*, 675–684. https://doi.org/10.1016/j.ijheatmasstransfer.2017.09.028

Yakubu, R. O., Mensah, L. D., Quansah, D. A., Adaramola, M. S., & Hammed, Y. (2022). Performance evaluation of bifacial solar PV modules under different climatic regions in Nigeria. *E3S Web of Conferences*, *354*, 02006. https://doi.org/10.1051/e3sconf/202235402006

Yield, E., & Estate, C. R. (2010). *Master Dissertation*. *September*, 2009–2010.